

QUASICRYSTAL STRUCTURE AND PROPERTIES¹

Alan I. Goldman

Ames Laboratory—US Department of Energy and Department of Physics,
Iowa State University, Ames, Iowa 50011

Mike Widom

Department of Physics, Carnegie Mellon University, Pittsburgh,
Pennsylvania 15213

KEY WORDS: Fibonacci, icosahedron, Penrose tiling, quasiperiodicity

1. INTRODUCTION

Quasicrystals possess long-range positional order, but noncrystallographic orientational order. Since 1984, when Shechtman and coworkers (1, 2) discovered icosahedral order in rapidly quenched Al_6Mn , the field has blossomed into an active subject of research in metallurgy, crystallography, and condensed matter physics. Much of the work done to date, and the main focus of this review concerns the problem of quasicrystal structure. Although important open questions in this area remain, we now understand many fundamental structural principles. For example, it is now well established that equilibrium quasicrystal phases exist, and that they possess long-range quasiperiodic translational order.

One cannot yet specify the location of each atom; however, much is known about the description of the structures. First, the recognition that related crystalline compounds consist of interpenetrating atomic clusters

¹ The US Government has the right to retain a nonexclusive, royalty-free license in and to any copyright covering this paper.

with icosahedral symmetry packed into a crystal lattice motivates cluster-based quasicrystal models, which describe local order over distances of tens of angstroms. Experiments utilizing both electron and tunneling (STM) microscopy verify the presence of such clusters in quasicrystals, as well. In this review, we show both experimental electron microscopy and STM data and some of the theoretically proposed clusters. To describe the long-range structure, we must deal with the quasiperiodic nature of the ordering. We accomplish this through analysis of related, periodic structures in a six-dimensional space. The higher dimensional description of quasicrystalline structures follows directly from the more familiar treatment of simple incommensurate structures. The three-dimensional icosahedral quasicrystal may be derived from a six-dimensional hypercubic lattice with its associated atomic basis. Elegant analysis of scattering data reveals the six-dimensional "atomic" basis directly. The true three-dimensional quasicrystal structure is simply a cut through this six-dimensional crystal.

Explaining why a given material forms a quasicrystal, instead of a more conventional crystal structure, proves more difficult. A phenomenological approach, based on quantum structural diagrams, successfully predicted new quasicrystal-forming compounds. But, predictions from first principles remain elusive. There is evidence that energetic effects, such as atomic sizes and chemical bonding, and entropic effects, which arise from structural rearrangements, all play essential roles.

Many other review articles about quasicrystals exist. Foremost is a series of books called *Aperiodicity and Order* (3–5); each volume contains several review articles about quasicrystals, incommensurate structures, and related topics. "Bond Orientational Order in Condensed Matter Systems" (6) contains relevant sections, as well. See also *Quasicrystals: The State of the Art* (7) for a collection of recent reviews. Henley's 1987 review article (8) includes an excellent bibliography. Many early papers in the field are collected in a single book (9). Invited papers in conference proceedings (10–14) serve well as reviews of specific topics.

This paper begins by discussing diffraction patterns with icosahedral symmetry. We distinguish between "simple icosahedral" and other icosahedral space groups, and then describe some quasicrystals with decagonal and other orientational symmetries. Next, quasicrystal structure in real space is examined through both experimental techniques of microscopy and through a theoretical description in six-dimensional space. After describing important classes of structural models, we include a section on theoretical and experimental studies of the electronic, magnetic, and vibrational properties of quasicrystals.

2. DIFFRACTION PATTERNS OF QUASICRYSTALLINE ALLOYS

2.1 *Icosahedral Symmetry*

Icosahedral phases arise in many pseudobinary and ternary metallic alloys by rapid quenching from the melt (1, 15), low temperature heat treatment of glassy ribbons (16) and thin films (17), and ion beam alloying techniques (18). The first icosahedral phase alloy was observed in transmission electron microscope studies of rapidly quenched alloys of Al_6Mn (1, 2). The composition of the icosahedral phase actually is closer to Al_4Mn (19), and the addition of a few atomic % Si stabilizes the icosahedral phase, thus leading to larger grain size and sharpened diffraction peaks (20, 21). The list of systems that form icosahedral phases at some composition now includes many other Al-M and Al-M-Si alloys (15), Al-Mg-Zn (22, 23), Al-Li-Cu (24, 25), Al-Cu-M (M = Mn, Fe, Ru, Cr, Os, V) (26), $\text{Ti}_2\text{-M}$ and Ti-M-Si alloys (M = Mn, Co, Cr, Ni and Fe) (27–31), Ga-Mg-Zn (32), and U-Pd-Si (16).

Experiments on the nucleation, growth, and recrystallization of quasicrystals have been reviewed by Kelton (33) and Schaefer & Bendersky (34). In the Al-Mn system, the glassy phase appears as microquasicrystalline, with grain sizes on the order of 25 Å (35). The glassy-to-icosahedral transformation proceeds by grain coarsening, rather than by nucleation and growth (36, 37). In contrast, similar studies of the “requasicrystallization” of U-Pd-Si (16, 38) and Al-Cu-V (39, 40) report that the transformation proceeds via nucleation and growth. Both the formation of the icosahedral phase and the details of quasicrystalline-to-crystalline transformations remain poorly understood.

With only a few notable and important exceptions, the icosahedral phases transform to ordinary crystalline phases upon heat treatment, thus showing that they are metastable. The discovery (24–26, 32) of stable icosahedral phases in Al-Li-Cu, Ga-Mg-Zn, and Al-Cu-M (M = Fe, Ru) allows the use of conventional equilibrium growth techniques to produce relatively large (0.1–5 mm) single grains of the icosahedral phase in these systems. Proper growth conditions (41–44) produce submillimeter-faceted single grains (Figure 1). Positional correlation lengths revealed by x-ray diffraction reach the scale of microns (45).

Figure 2 displays electron diffraction patterns perpendicular to the high symmetry twofold, threefold, and fivefold directions in icosahedral Al-Mn, thus illustrating several key features characteristic of all quasicrystalline diffraction patterns. First, the point group of quasicrystalline structures contains noncrystallographic rotational symmetries. Selected area diffrac-

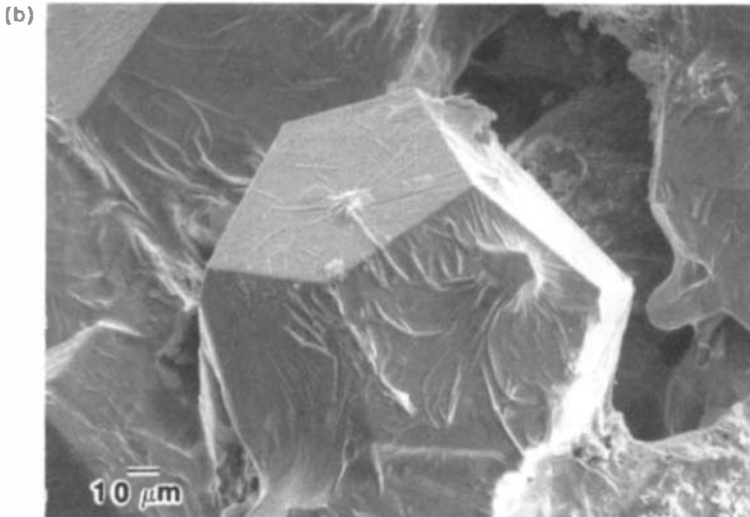
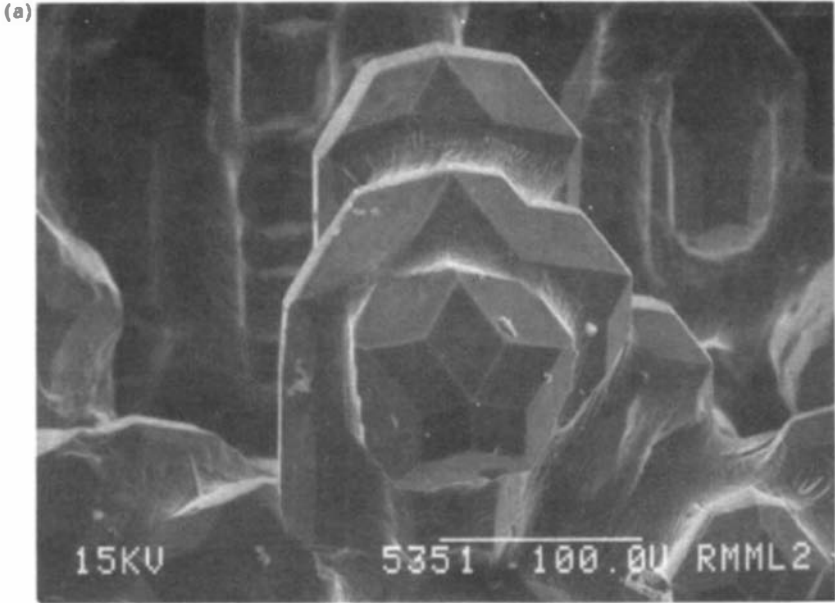


Figure 1 (a) Single grains of icosahedral Al-Li-Cu displaying facets in the shape of rhombic triacontahedra. (b) Pentagonal dodecahedra of Al-Cu-Fe. (Courtesy of F. W. Gayle.)

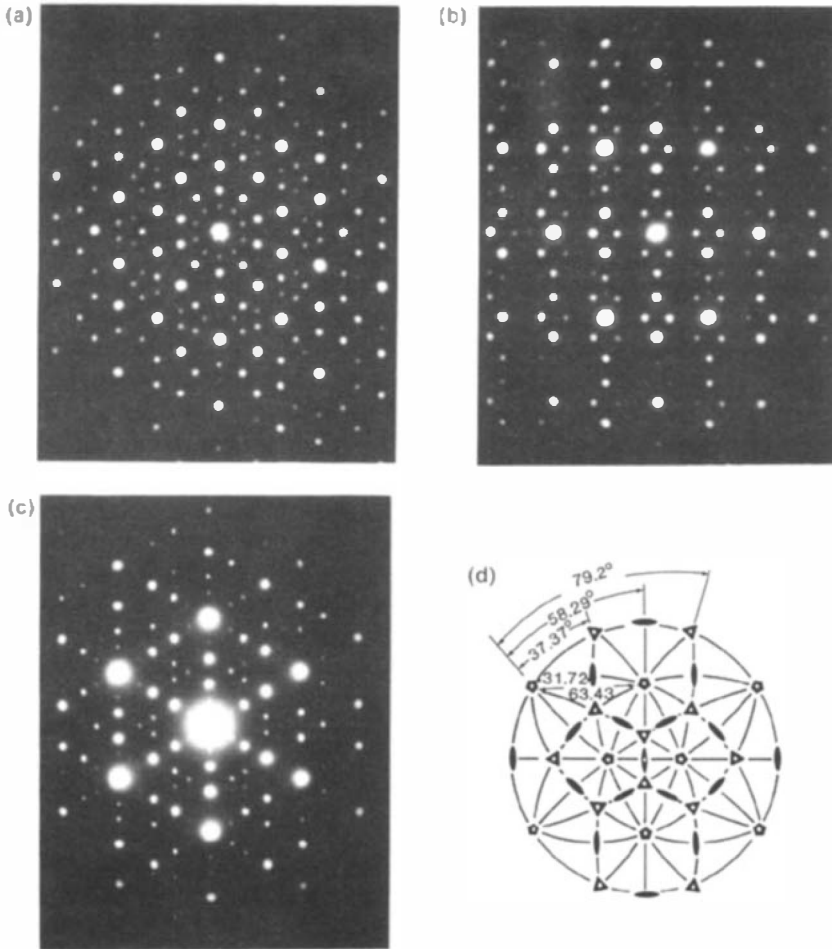


Figure 2 Electron diffraction patterns of icosahedral Al-Mn taken along the (a) fivefold, (b) twofold, and (c) threefold axes. (Courtesy of K. Kelton.) The angular relationship between these high symmetry directions is evident in the stereographic projection in (d).

tion patterns pass through a sequence of twofold, threefold, and fivefold axes characteristic of icosahedral symmetry, as grains are rotated through the angles of the icosahedral point group (Figure 2d). The fivefold zone axis (Figure 2a) for the icosahedral group $m\bar{3}\bar{5}$ is inconsistent with long-range periodic translational order (46). The presence of well-defined diffraction spots in these patterns, however, points to the presence of some form of long-range positional order. Indeed, in several instances the diffraction peaks from quasicrystals are as sharp as those found in the

diffraction patterns from high-quality periodic crystals of metallic alloys (45, 47), with peak widths limited by experimental resolution.

For a periodic crystal, the position of any diffraction peak in the reciprocal lattice obeys

$$\mathbf{G} = h\mathbf{a} + k\mathbf{b} + l\mathbf{c}, \quad 1.$$

where the integers (h, k, l) are the Miller indices of the diffraction peak. The size and symmetry of the unit cell determine the reciprocal lattice basis vectors $(\mathbf{a}, \mathbf{b}, \mathbf{c})$. The ratio of the lengths of reciprocal lattice vectors, \mathbf{G}_1 and \mathbf{G}_2 , for any two collinear diffraction peaks from a periodic crystal must be a ratio of integers (a rational number).

Careful inspection of the twofold, threefold, and fivefold electron diffraction patterns in Figure 2, however, reveals irrational ratios among collinear spots. For instance, the fivefold plane of Figure 2a contains five sets of twofold axes 72° apart. Along these twofold axes, the sequence of bright diffraction spots follows the integer powers of the golden mean [$\tau = (\sqrt{5} + 1)/2$], an irrational number that arises in the geometry of icosahedra and pentagons. Similarly, sequences of bright spots along the fivefold and threefold axes (seen in the twofold plane of Figure 2b) remain invariant under multiplication or division by τ^3 . The entire diffraction pattern, therefore, appears the same under τ^3 self-similarity transformations (48).

We must choose a suitable set of basis vectors and a fundamental length scale to index the diffraction pattern from icosahedral alloys. For icosahedral structures, it seems most appropriate to choose a set of basis vectors that emphasize the underlying icosahedral symmetry of the structure, as shown in Figure 3. Unit vectors point along six independent vertex directions of the icosahedron in the "umbrella convention" described by Elser (49). All diffraction spots in Figure 2 can then be indexed by sets of six Miller indices, $(n_1, n_2, n_3, n_4, n_5, n_6)$, such that

$$\mathbf{G} = G_0 \sum_i n_i \hat{\mathbf{q}}_i, \quad 2.$$

where

$$\begin{aligned} \hat{\mathbf{q}}_1 &= \gamma(1, \tau, 0), & \hat{\mathbf{q}}_2 &= \gamma(\tau, 0, 1) \\ \hat{\mathbf{q}}_3 &= \gamma(\tau, 0, -1), & \hat{\mathbf{q}}_4 &= \gamma(0, 1, -\tau) \\ \hat{\mathbf{q}}_5 &= \gamma(-1, \tau, 0), & \hat{\mathbf{q}}_6 &= \gamma(0, 1, \tau), \end{aligned} \quad 3.$$

and $\gamma = (\tau^2 + 1)^{-1/2}$. This particular choice of six vertex vectors differs from, but is completely equivalent to, the original indexing scheme used by Bancel et al (50).

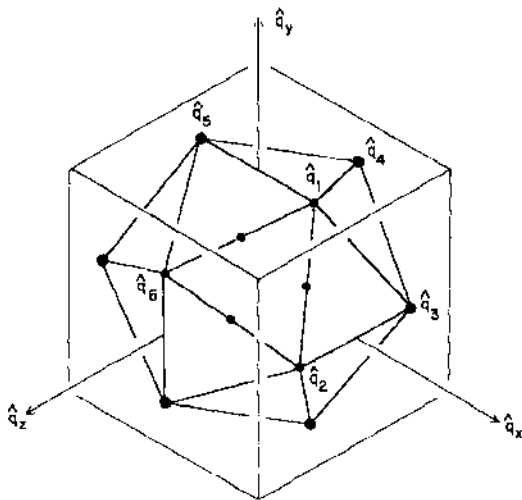


Figure 3 Reciprocal lattice basis vectors used for indexing the icosahedral phase diffraction peaks.

A second complementary set of reciprocal lattice vectors arises as a consequence of the incommensurability of the structure (48, 51–57). Each diffraction peak is associated with both a physical momentum coordinate \mathbf{G} , and its dual, or “phason” momentum coordinate,

$$\mathbf{G}_\perp = G_0 \sum_i n_i \hat{\mathbf{q}}_i^\perp. \quad 4.$$

The basis vectors used for constructing \mathbf{G}_\perp derive from permutations of the $\hat{\mathbf{q}}$ -vectors in Figure 3:

$$\begin{aligned} \hat{\mathbf{q}}_1^\perp &= -\hat{\mathbf{q}}_1, & \hat{\mathbf{q}}_2^\perp &= \hat{\mathbf{q}}_2 \\ \hat{\mathbf{q}}_3^\perp &= \hat{\mathbf{q}}_4, & \hat{\mathbf{q}}_4^\perp &= \hat{\mathbf{q}}_6 \\ \hat{\mathbf{q}}_5^\perp &= \hat{\mathbf{q}}_3, & \hat{\mathbf{q}}_6^\perp &= \hat{\mathbf{q}}_5. \end{aligned} \quad 5.$$

Phason momentum plays an important role in the determination of diffraction peak intensities and the description of disorder in these materials (17, 51, 58–60). We discuss phason disorder in detail in Section 3.3.

Other indexing schemes for the icosahedral phase are possible. For instance, choose a set of three orthogonal basis vectors $(\hat{\mathbf{q}}_x, \hat{\mathbf{q}}_y, \hat{\mathbf{q}}_z)$ parallel to three twofold axes of the icosahedron in Figure 3. The incommensurability of the structure requires that each reciprocal lattice point

be labeled by a set of Miller indices (h, k, l) , which are irrational numbers. A second indexing scheme, introduced by Cahn et al (61), employs three pairs of integer indices to label diffraction peaks by using the $(\hat{\mathbf{q}}_x, \hat{\mathbf{q}}_y, \hat{\mathbf{q}}_z)$ basis vectors. We can denote diffraction peaks by $(h/h', k/k', l/l')$, where $h/h' \equiv h + h'\tau$, $k/k' \equiv k + k'\tau$, $l/l' \equiv l + l'\tau$. A simple formula

$$\begin{aligned} h &= n_1 - n_5 & h' &= n_2 + n_3 \\ k &= n_4 + n_6 & k' &= n_1 + n_5 \\ l &= n_2 - n_3 & l' &= n_6 - n_4 \end{aligned} \quad 6.$$

relates the two indexing systems. Although both indexing systems offer certain advantages for the description of diffraction patterns from the icosahedral alloys, we employ the former in the remainder of this article, because it emphasizes the underlying icosahedral symmetry of the structure.

The intrinsic incommensurability of the structure complicates the choice of a fundamental length scale with which to set G_0 for quasicrystals. Bragg peaks densely fill reciprocal space, so there is no minimum separation between diffraction peaks, which may be used to set reciprocal space length scales. However, as seen in Figure 2, the vast majority of these diffraction peaks are of such low intensity that they are indistinguishable from the background. Our choice of basis vectors $\hat{\mathbf{q}}_i$ limits plausible candidates for G_0 to diffraction peaks along the vertex, or fivefold, directions. However, an interesting implication of the τ^3 invariance of the diffraction patterns shown in Figure 2 is that the fundamental length scale, or "quasilattice constant," of the structure can only be determined from diffraction measurement to within a factor of τ^3 . One choice of a fundamental reciprocal lattice vector yields a length scale on the order of interatomic distances, whereas other choices come closer to distances between clusters of atoms. In the case of the Al-Mn-Si icosahedral alloy, Bancel et al (50) assigned the fundamental (100000) reciprocal lattice vector to the bright spot along the fivefold axis at $Q = 2.894 \text{ \AA}^{-1}$. With this choice, all peaks in the powder diffraction pattern indexed with the smallest number of nonzero integer indices. Another choice for the fundamental reciprocal lattice vector in Al-Mn-Si is the relatively weak peak along the fivefold axis at $Q = 0.68 \text{ \AA}^{-1}$. This value differs from the previous value by a factor of τ^{-3} . Many researchers favor this choice, because it represents a length scale in real space, which is close to the rhombohedral edge lengths in tiling models for the icosahedral phase (48, 61, 62) and the closely related cubic α -Al-Mn-Si phase (63, 64).

Let's make some general observations about indexing of icosahedral quasicrystals. The set of icosahedral basis vectors $\{\hat{\mathbf{q}}_i\}$ is incommensurate

because no single basis vector can be represented as a linear combination with integer coefficients of the remaining five. Therefore, we need more integer Miller indices than we have spatial dimensions. Just as the set of all Bragg peaks labeled by three integer Miller indices forms a crystal lattice in three-dimensional reciprocal space, so the set of all Bragg peaks labeled by six integers ($n_1, n_2, n_3, n_4, n_5, n_6$) is geometrically equivalent to lattice in six-dimensional reciprocal space. The reciprocal lattice defined by taking all combinations of three integers is simple cubic. Accordingly, the reciprocal lattice defined by taking all combinations of six integers is “simple hypercubic.” Icosahedral quasicrystals, whose reciprocal lattices are simple hypercubic, are called “simple icosahedral.”

Three different “quasi-Bravais” lattices contain icosahedral point group symmetry—“face centered icosahedral” (FCI) and “body centered icosahedral” (BCI)—in addition to the simple icosahedral (SI) structure, whose diffraction pattern (reciprocal lattice) we described above (65). The differences between the three icosahedral quasi-Bravais lattices appear most clearly in reciprocal space. The reciprocal lattice of a simple icosahedral quasicrystal, the set of all combinations of six Miller indices, is equivalent to a simple hypercubic lattice in six dimensions. Now consider, instead of all combinations of Miller indices, only those obtained by adding basis vectors \hat{q}_i in pairs. The resulting lattice in reciprocal space contains only points for which $\sum n_i$ is even. By analogy with three dimensions, we call this a face-centered hypercubic reciprocal lattice. Icosahedral quasicrystals with such a reciprocal lattice are, therefore, body-centered icosahedral. If we instead consider the reciprocal space lattice of diffraction peaks labeled by Miller indices, which are either all even or all odd, we obtain by analogy a body-centered hypercubic reciprocal lattice corresponding in real space to a face-centered icosahedral quasicrystal.

The classification of noncrystallographic space groups (65–67) is physically illuminating, as well as mathematically elegant. One finds that the three quasi-Bravais lattices described above are the only ones possible with icosahedral symmetry. Other noncrystallographic space groups exist in three dimensions with axial symmetries. These have noncrystallographic symmetry (such as eightfold, tenfold, or twelvefold rotations) around a single axis, but the reciprocal lattice is periodic along this axis (note that the structure itself need not be periodic). There are even structures whose reciprocal lattices reveal periodicity in two-dimensions and quasiperiodicity along the remaining one.

Although BCI alloys have never been observed, the Al-Cu-M alloys discovered by Tsai et al (26) yield diffraction patterns (Figure 4) that classify them as FCI alloys. In particular, the sequence of bright diffraction spots along the threefold and fivefold axes in the twofold plane (Figure

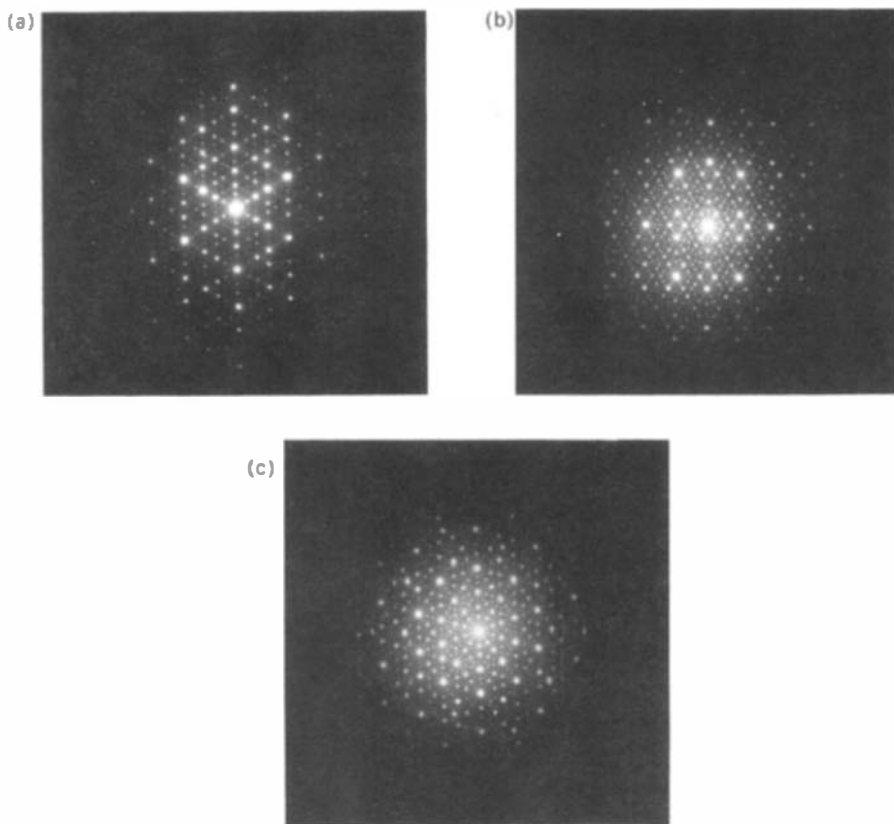


Figure 4 Electron diffraction patterns of FCI Al-Cu-Fe taken along the (a) fivefold, (b) twofold, (c) threefold axes. (Courtesy of S. Ebalard and F. Spaepen.)

4b) are related by factors of τ , rather than τ^3 . The entire diffraction pattern is invariant under multiplication or division by τ ; therefore, G_0 is only determined to within a factor of τ . The FCI structure apparently results from chemical ordering of the atoms on an SI quasilattice, analogous to superlattice ordering in crystalline alloys, such as β -brass. For example, electron microscopy studies establish the presence of antiphase domains characteristic of chemical ordering in FCI Al-Cu-Fe (68, 69). The antiphase domains disappear upon heat treatment, which evidently increases the range of chemical order. Interestingly, it seems that very short range FCI chemical order exists in SI alloys because diffuse scattering at FCI superlattice positions appears in the SI alloys Al-Mn-Si (70, 71) and Al-Li-Cu (72). Changing the Al/Pd composition in Al-Pd-Mn icosahedral alloys (73) drives a transformation between the SI and FCI structures.

One of the most fascinating differences between the SI and FCI alloys is the ubiquitous disorder revealed in the x-ray diffraction patterns of the former, and its absence in the latter. The particular type of disorder, termed “phason strain” (see Section 3.3) found in the SI alloys is peculiar to quasicrystals and other incommensurate structures. Broadening of diffraction peaks in powder patterns, or peak shifts and distortions in single grain diffraction studies (15, 17, 58–60), whose magnitude depends on G_{\perp} , signal the presence of phason strain. Explaining the absence of such strains in FCI alloys remains an important open problem.

The presence of significant diffuse scattering for many SI systems (28, 70, 72, 74–76) deserves special mention. These patterns (Figure 5) are most clearly seen, and have been studied extensively in Ti-Mn (77, 78). The origin of this diffuse scattering is still a matter of some controversy. In certain cases, the appearance of diffuse scattering at the SI forbidden, but FCI allowed, Bragg points has been interpreted in terms of short-range chemical order characteristic of the FCI structure (70, 71). Similar patterns of diffuse scattering arise naturally from structural models for the icosahedral phase that contain significant disorder (72, 79–81). On the other

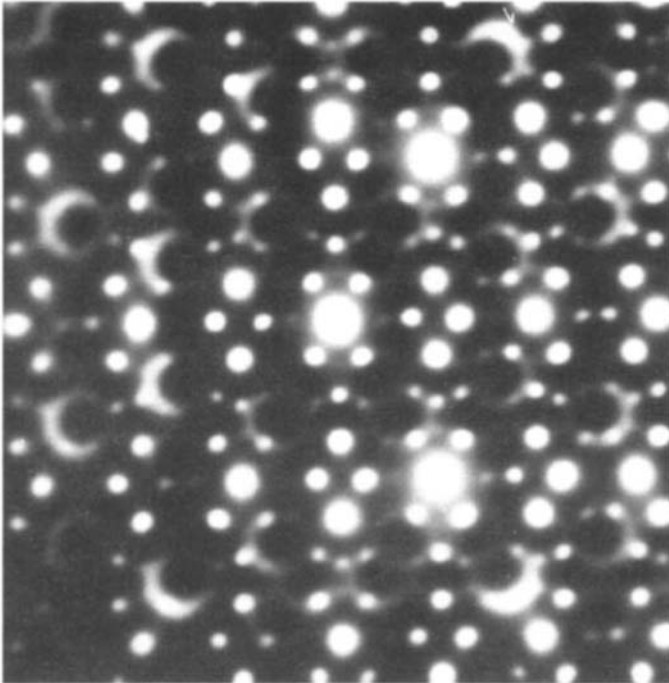


Figure 5 Diffuse scattering pattern of icosahedral Ti-Mn (courtesy of K. F. Kelton).

hand, similar patterns of diffuse scattering occur in crystalline alloys, which share structural building blocks (icosahedral atomic clusters) with the icosahedral phase, thus suggesting that the diffuse scattering arises from positional or chemical ordering in these structural units themselves (82).

2.2 Decagonal and Other Symmetries

Examples of many of the other noncrystallographic space groups (65, 66) have also been reported. The decagonal phase (or T-phase) was first observed, but not identified as such, in rapidly quenched alloys of Al-Mn and Al-Pd (83, 84). Bendersky (85) and Chattopadhyay et al (86) later identified the Al-Mn alloy as a quasicrystal and noted its close relationship to the icosahedral phase in this system. The decagonal phase is intermediate between the crystalline and icosahedral phases. In Al-Mn, the decagonal phase forms along with the icosahedral phase when Mn concentrations exceed 16 atomic %. At higher Mn concentrations and/or slower quench rates, the decagonal phase forms instead of the icosahedral phase (87, 88), while the nucleation of the decagonal phase in Al-Mn decreases with the addition of a few % Si (21).

Many other binary Al-M alloys, ($M = \text{Fe, Co, Ni, Ru, Rh, Pd, Os, Ir, and Pt}$), as well as ternary alloys with and without Al (89, 90), display decagonal phases. With a few notable exceptions, the decagonal alloys are metastable, although the recrystallization temperatures exceed those for the icosahedral phase. Recently, stable decagonal phases were discovered in Al-Cu-Co and Al-Cu-Co-Si alloys (91, 92). Millimeter-sized grains with a decaprismatic morphology grow by slowly cooling ingots from the melt (Figure 6).

Quasiperiodic diffraction patterns with tenfold symmetry in a plane and translational periodicity along the axis perpendicular to that plane (Figure 7) characterize the decagonal alloys. Ten equivalent twofold directions (labeled D), appear 90° from the tenfold axis and 36° from each other. Another set of twofold directions (labeled P) lie in the plane 18° away from the D axes. The point symmetry of the decagonal phase is $10/mmm$, and the absence of odd-order spots along the P direction are the extinctions expected for the space group $P10_5/mmc$ (65, 93).

Diffraction patterns from the decagonal phase index to a set of pentagonal bipyramid basis vectors related to the icosahedral basis vectors described above (94, 95). If we distort the five vertex vectors \hat{q}_2 through \hat{q}_6 , so that their projection along \hat{q}_1 becomes a rational fraction of \hat{q}_1 , this "squashed icosahedron" emphasizes the relationship between the icosahedral and decagonal diffraction patterns. While a simple distortion relates the reciprocal space basis vectors, such a simple relation need not hold in real space. Decagonal symmetry, with its tenfold axis, is not a

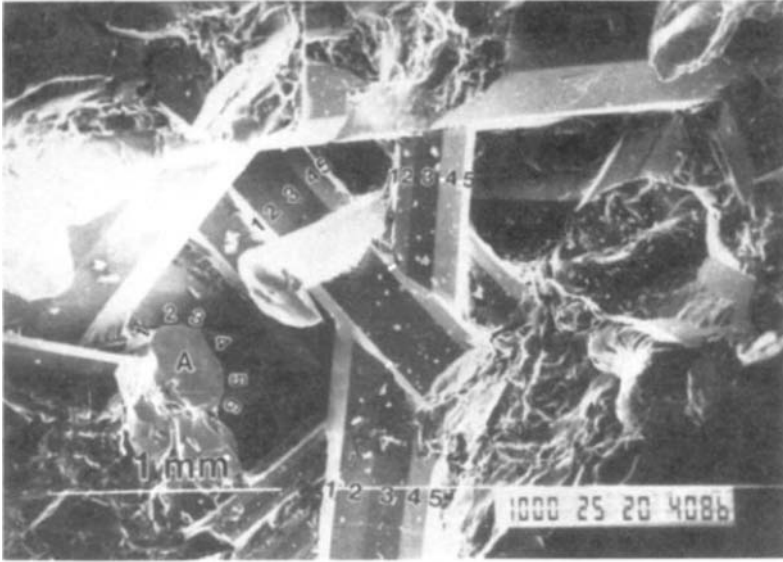


Figure 6 Decaprisymmetric single grains of Al-Cu-Co-Si. (Courtesy of L. X. He.)

subgroup of icosahedral symmetry. To transform icosahedral structures into decagonal structures one must break the icosahedral symmetry (as described above) and also introduce a mirror plane perpendicular to the fivefold axis (96).

An alternative, and more frequently used, indexing scheme for the decagonal phase employs five coplanar basis vectors, 72° apart, along with a sixth vector perpendicular to the plane (90, 97, 98). The physical and phason components of the reciprocal lattice vectors are then

$$\mathbf{G} = \sum_{i=0}^5 n_i \mathbf{q}_i, \quad \mathbf{G}_\perp = \sum_{j=0}^5 n_j \mathbf{q}_j^\perp, \tag{7}$$

where

$$\mathbf{q}_i = q_p * \left[\hat{\mathbf{x}} \cos\left(\frac{2\pi i}{5}\right) + \hat{\mathbf{y}} \sin\left(\frac{2\pi i}{5}\right) \right], \quad (i = 0 \rightarrow 4)$$

$$\mathbf{q}_5 = q_z \hat{\mathbf{z}}, \tag{8}$$

and

$$\mathbf{q}_j^\perp = \mathbf{q}_{2j \bmod 5} \quad (j = 0 \rightarrow 4). \tag{9}$$

Here, q_p and q_z denote the fundamental reciprocal lattice vectors in the

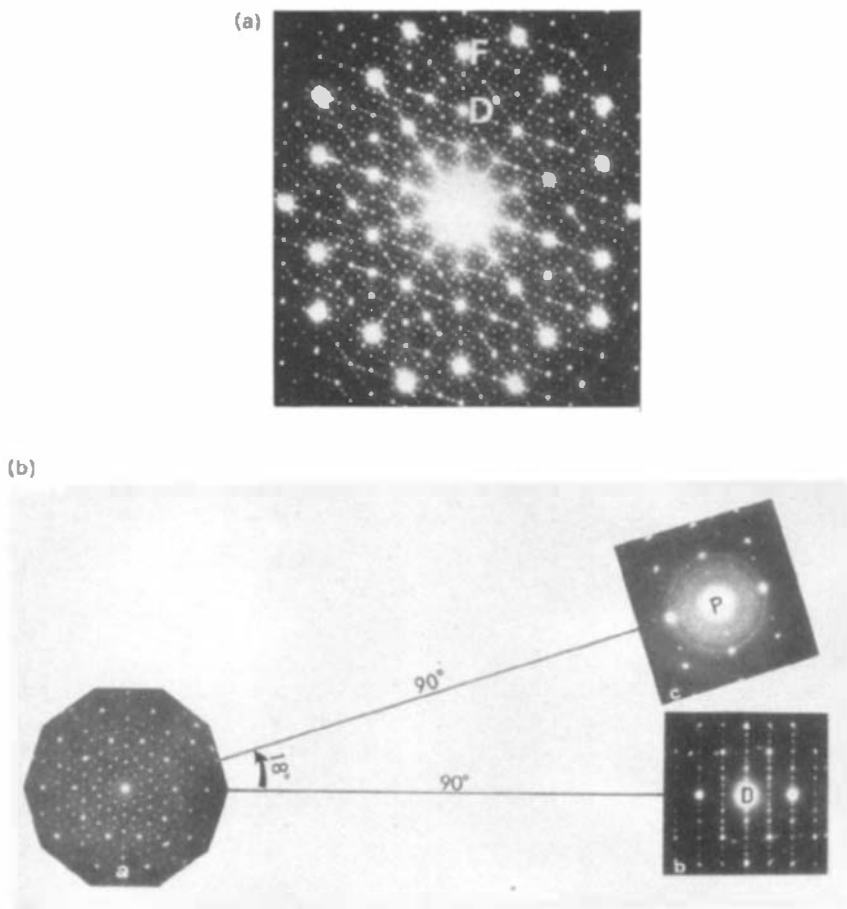


Figure 7 (a) The tenfold diffraction plane of decagonal Al-Cu-Co-Si. Peak F is at τ times peak D. (b) The orientational relation between the tenfold axis and twofold P and D axes in decagonal phase alloys. (Courtesy of L. X. He.)

quasiperiodic plane and along the periodic direction, respectively. The tenfold diffraction pattern in Figure 6 remains invariant under multiplication or division by τ . Therefore, the choice of η_p is ambiguous within factors of τ . We can actually label each diffraction peak with five, rather than six, indices (four in-plane, one out-of-plane), because the five vectors that point to the vertices of a pentagon are not linearly independent. This causes some confusion, as any reciprocal lattice point may be labeled by six different, but equivalent, sets of indices. Mukhopadhyay et al (99) suggest a least path criterion, by which one selects the set of indices that yields the minimum sum.

Icosahedral and decagonal phase diffraction patterns share a close relationship (85, 100). One of the six fivefold axes of the icosahedral phase becomes the tenfold axis of the decagonal phase, while the other fivefold and threefold axes disappear. We see pseudo two-, three-, and fivefold patterns if we tilt grains of decagonal phase by appropriate angles (31.72° , 37.37° , and 63.43° , respectively) away from the tenfold axis along the P directions.

Several periodicities, all related to a basic repeat distance (101) of about 4 \AA occur along the tenfold axis for all systems studied to date. For instance, in Al-Mn, the periodicity along the tenfold axis is 12.4 \AA , whereas it is 16.5 \AA in Al-Fe and Al-Pd, and it is close to 4 \AA in Al-Ni. In the Al-Cu-Co decagonal phase, repeat distances of about 4, 8, 12, and 16 \AA along the periodic direction appear under different conditions in the same alloy (91). Indeed, streaking and diffuse scattering characterize the diffraction patterns of all decagonal phase alloys, which suggests the presence of stacking faults and polytypism.

Other, noncrystallographic axial quasicrystals, with eightfold and twelfold rotational symmetry, have been reported. Wang et al (102) first reported octagonal quasicrystals in Cr-Ni-Si, V-Ni-Si, Mn-Si, Mo-Ni-Si, Mn-Fe-Si, and Mn-Al-Si. In all of these systems, the octagonal phase coexists with microtwins of the cubic β -Mn structures (103). Convergent beam electron diffraction (CBED) patterns and high-resolution lattice images differentiate between these microtwins and the true octagonal phase. Quasicrystals with dodecagonal symmetry are reported in V-Ni and V-Ni-Si alloys (104), as well as laser-vaporized and later condensed particles of Cr-Ni (105). For brief reviews of the experimental progress on these quasicrystals, see the articles by Kuo (106, 107). In these reports, however, these quasicrystals occur only in the presence of twinned crystal phases, which raises doubts whether they are true bulk phases. In addition, twinned conventional crystals may easily mimic eight- and twelfold diffraction patterns to high accuracy (108, 109).

He et al (110) report the existence of a one-dimensional incommensurate structure in rapidly quenched alloys of Al-Ni-Si, Al-Cu-Mn, and Al-Cu-Co that may be structurally related to quasicrystals. These alloys exhibit periodic diffraction patterns along two directions (the tenfold and P axes of the decagonal phase), but quasiperiodic patterns along the third direction (one of the decagonal D axes). This phase may be related to the crystalline τ -phases observed in Al-Ni-Cu (111, 112) alloys. The τ -phases are a series of vacancy-ordered distorted CsCl structures with repeat units along the [111] directions that approximate a Fibonacci sequence. So far τ_2 , τ_3 , τ_5 , τ_8 , and τ_{13} variants (where the subscript denotes the number of layers in the repeat unit) have been identified. The one-dimensional Fibonacci quasicrystal is τ_n in the limit $n \rightarrow \infty$.

3. REAL SPACE STRUCTURE

3.1 *Microscopy*

Fourier inversion of the electron diffraction patterns to obtain images of the real space density is an important technique for the study of quasicrystals. Electron microscopy recombines a subset of the diffraction spots from some area of the sample at the image plane, thus producing an image with atomic scale ($\approx 2 \text{ \AA}$) lateral resolution. The optical system of the microscope performs the transform, thereby preserving both intensity and phase information. On the other hand, one must not interpret the light and dark regions of the images in terms of positions of individual atoms. The image itself results from multiple scattering of electrons through the entire thickness (typically on the order of 100 \AA) of the sample. Furthermore, subtle changes in the imaging process (e.g. defocusing) can produce global shifts in the contrast of the images. No single high-resolution lattice image tells the entire story, and it is dangerous to support or denounce any particular structural model for quasicrystals solely upon these images (113, 114).

Even with the above-stated disclaimers, lattice imaging proves very useful for investigations of structure, defects, and strain in crystalline materials. Many groups now also apply this technique to quasicrystalline alloys (115–118). Figure 8 compares high-resolution lattice images taken (a) along the fivefold axis of icosahedral Al-Mn (119), and (b) the tenfold axis of decagonal Al-Cu-Co-Si (L. X. He, private communication), with a simulated image (c) of the same plane produced by the density wave expansion

$$\rho(\mathbf{r}) = \sum_{i=1}^5 \cos(\mathbf{G}_i \cdot \mathbf{r}). \quad 10.$$

\mathbf{G}_i are equally spaced around a circle (separated by 72°). Although the simulation includes \mathbf{G}_i of only a single magnitude, real lattice images typically make use of several Fourier components (rings of diffraction spots) out to some cutoff G_{\max} limited by aberrations. Simulated lattice images, therefore, contain less detail than real ones. Nevertheless, both the experimental and simulated images share common features, such as local regions of tenfold symmetry. A clever experiment, in which five crossed laser beams were shone through a colloidal suspension of polystyrene spheres, created an artificial quasicrystal (120) based on Equation 10.

View Figure 8c at grazing incidence to see rows of contrast aperiodically spaced in a Fibonacci sequence along the five twofold directions. Closer

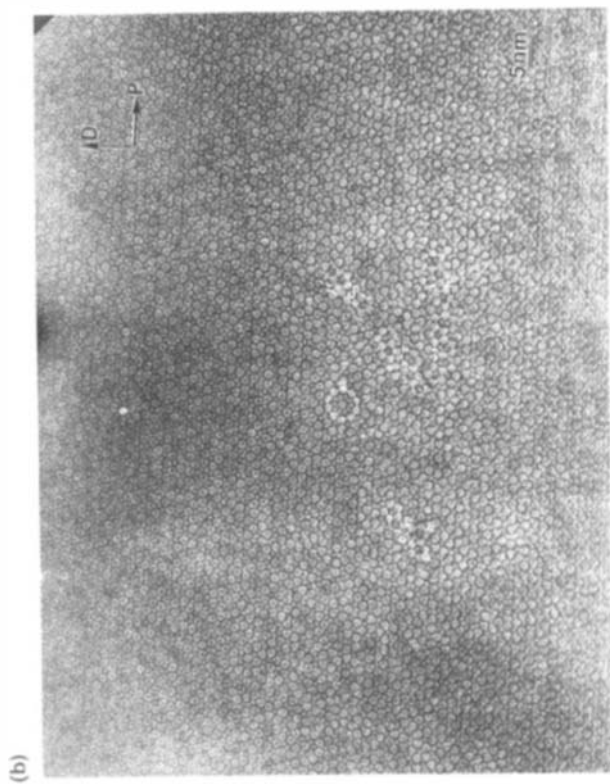
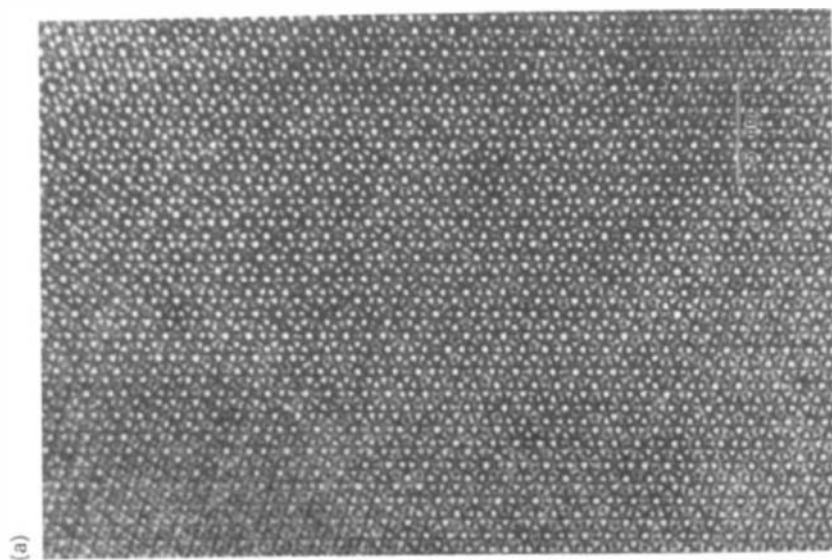
inspection of the lattice image Figure 8*a* reveals that the rows of contrast often shift discontinuously at points and then continue uninterrupted. Such jogs arise from the same long wavelength phason strain in quasicrystals (17, 58–60) that create broadening and shifting of diffraction peaks. In the equivalent fivefold plane lattice images of FCI Al-Cu-Fe (Figure 8*d*) these discontinuous shifts are all but absent (121). This is consistent with the absence of diffraction peak broadening in the x-ray patterns of the FCI alloys.

As mentioned above, light and dark spots in these lattice images represent an average of the electron density projected parallel to the incident beam direction through the sample. More recently, STM studies of the decagonal phase of Al-Cu-Co provided the first glimpse of true atomic scale structure within a single surface plane (122). Figure 9 reproduces the STM image of the quasiperiodic plane (perpendicular to the tenfold axis). Steps in the surface appear as jagged vertical lines running across the image. This figure clearly shows the preservation of relative orientation of the atomic structure from layer to layer. The image bears a striking resemblance to pentagonal quasilattices constructed by tiling models or density wave expansions, as well as the high resolution electron microscopy (HREM) lattice images of the tenfold plane of the decagonal phase (see Figure 8*b*).

Examination of Figures 8 and 9, as well as consideration of the known structures of presumably related crystal phases, suggests models for the local atomic structure of quasicrystal-forming compounds. Many crystal structures may be described in terms of icosahedrally symmetric clusters of atoms (123–133). For example, Figure 10*a* shows a cluster taken from the Bergman phase (123) of $\text{Mg}_{32}(\text{Al}, \text{Zn})_{49}$. By joining or overlapping these clusters, one can fill space in many ways, both periodically (as in the Bergman phase) and aperiodically (63, 64). Alternatively, one may decompose the clusters into “tiles,” such as those illustrated in Figure 10*b–d*. Again, these tiles may be arranged in many ways to fill space.

3.2 Hyperspace

We now ask theoretically how best to describe a structure that, due to its quasiperiodicity, never repeats itself. Our discussion of indexing quasicrystalline diffraction patterns emphasized the requirement for six Miller indices when the diffraction pattern has icosahedral symmetry. As an automatic by-product of this requirement, description of atomic structures of icosahedral materials is most conveniently conducted in six-dimensional space. Equation 2 gives the position of each peak in the diffraction pattern. Assuming that the Bragg peaks contain all the structural information (i.e. ignoring any diffuse scattering), we write the electron density



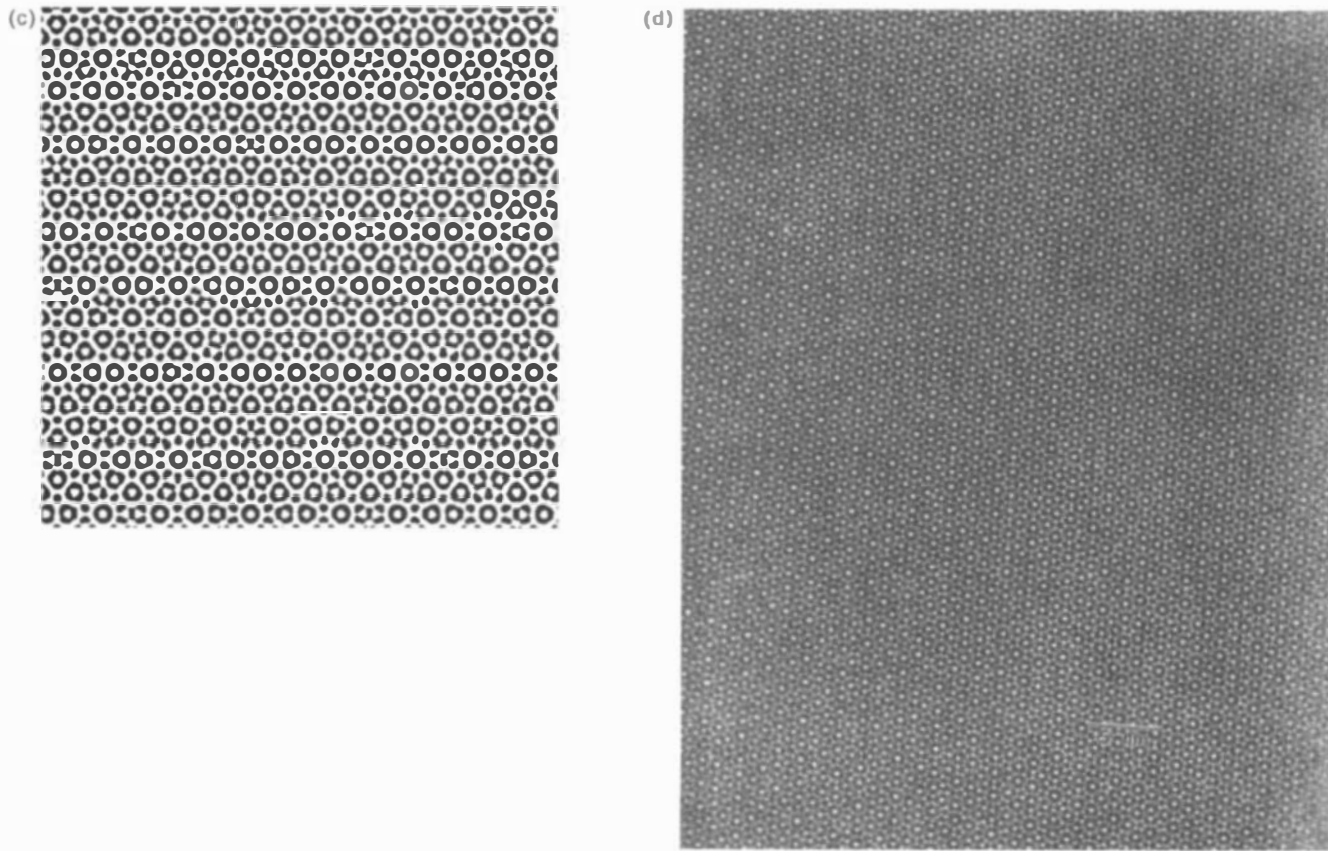


Figure 8 High-resolution lattice images taken along (a) the fivefold axis of Al-Mn-Si and (b) the tenfold axis of Al-Cu-Co-Si. White lines outline frequently occurring motifs. (c) A simulated density image as described in the text. (d) high-resolution lattice image taken along the fivefold axis of Al-Cu-Fe. (Figures a and d are courtesy of K. Hiraga, b is courtesy of L. X. He.)



Figure 9 STM image of the surface perpendicular to the tenfold axis of decagonal Al-Cu-Co. (Courtesy of A. R. Kortan.)

$$\rho(\mathbf{r}) = \sum_{\{n_i\}} A_{\{n_i\}} \cos \left\{ \sum_i (n_i \hat{\mathbf{q}}_i \cdot \mathbf{r} + \phi_{\{n_i\}}) \right\}, \quad 11.$$

where the coefficient $A_{\{n_i\}}$ represents the amplitude and $\phi_{\{n_i\}}$ represents the phase of the peak with Miller indices $\{n_i\}$. Figure 8c illustrates such a function for the simple case in which all phases vanish and $A_{\{n_i\}} = 0$, except for $\{n_i\} \in [1, 0, 0, 0, 0, 0]$.

Clearly, $\rho(\mathbf{r})$ is a periodic function of each combination $\hat{\mathbf{q}}_i \cdot \mathbf{r}$. In fact, we can express $\rho(\mathbf{r})$ in terms of a periodic function of six variables

$$\rho_6(\theta_1, \theta_2, \theta_3, \theta_4, \theta_5, \theta_6) \equiv \sum_{\{n_i\}} A_{\{n_i\}} \cos \left\{ \sum_i (n_i \theta_i + \phi_{n_i}) \right\}. \quad 12.$$

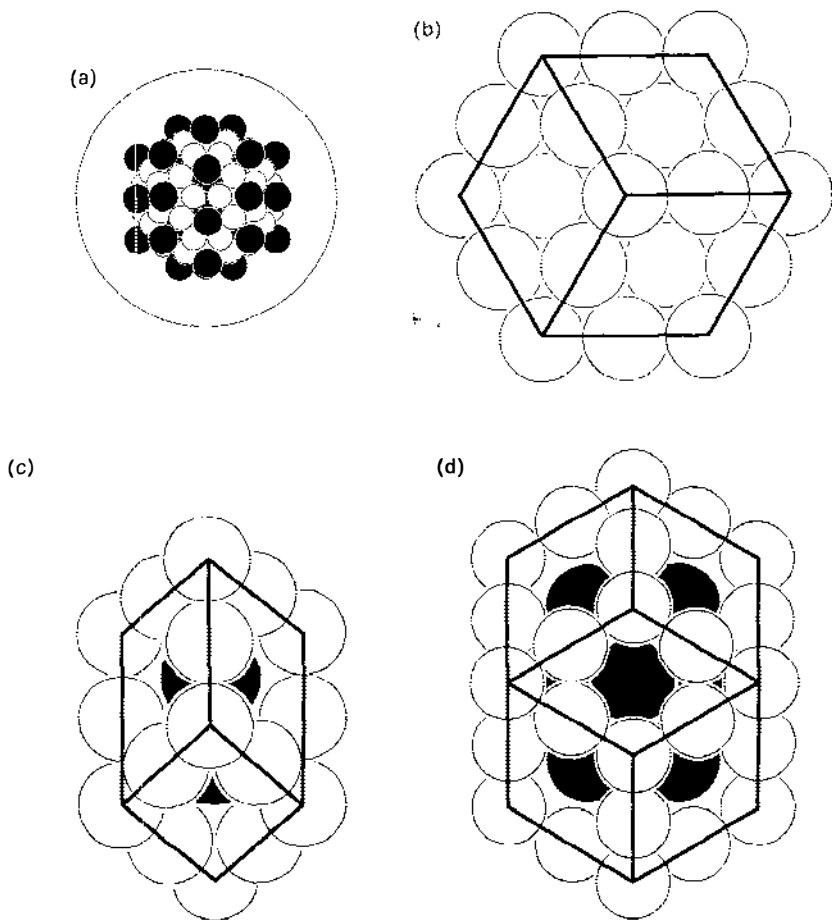


Figure 10 (a) Cluster of 73 Al and Zn atoms (white) and 64 Mg atoms (black) from $Mg_{32}(Al, Zn)_{49}$. (b) Decoration of tiles [oblate (b) and prolate (c) rhombohedra and a rhombic dodecahedron] with white and black atoms.

Now, a function of six variables may always be represented as a function in a six-dimensional space, in which each variable corresponds to one of the six orthogonal coordinates of the space. Then, we obtain the electron density expressed in Equation 11

$$\rho(\mathbf{r}) = \rho_6(\hat{q}_1 \cdot \mathbf{r}, \hat{q}_2 \cdot \mathbf{r}, \hat{q}_3 \cdot \mathbf{r}, \hat{q}_4 \cdot \mathbf{r}, \hat{q}_5 \cdot \mathbf{r}, \hat{q}_6 \cdot \mathbf{r}). \quad 13.$$

But, this is just a cross section of the function $\rho_6(\mathbf{r})$ on a three-dimensional

hyperplane in six-dimensional space. That is, we evaluate $\rho_6(\theta_1, \theta_2, \theta_3, \theta_4, \theta_5, \theta_6)$ only at points of the form $\{\hat{\mathbf{q}}_i \cdot \mathbf{r}\}$.

Figure 11a illustrates the connection between an atomic structure in real, physical space and a fictitious structure in hyperspace. For the purpose of illustration, we show atoms placed in a quasiperiodic one-dimensional sequence. The atomic positions are the intersections of the physical one-dimensional space labeled E with "atomic surfaces," which appear as line segments, placed in a two-dimensional square lattice with axes θ_1 and θ_2 . Atomic surfaces need not simply be line segments. They may bend in hyperspace and even join with surfaces in other unit cells. There is no restriction on the number of atomic surfaces in a unit cell. Altering the atomic surfaces alters the placement of atoms in physical space. The line

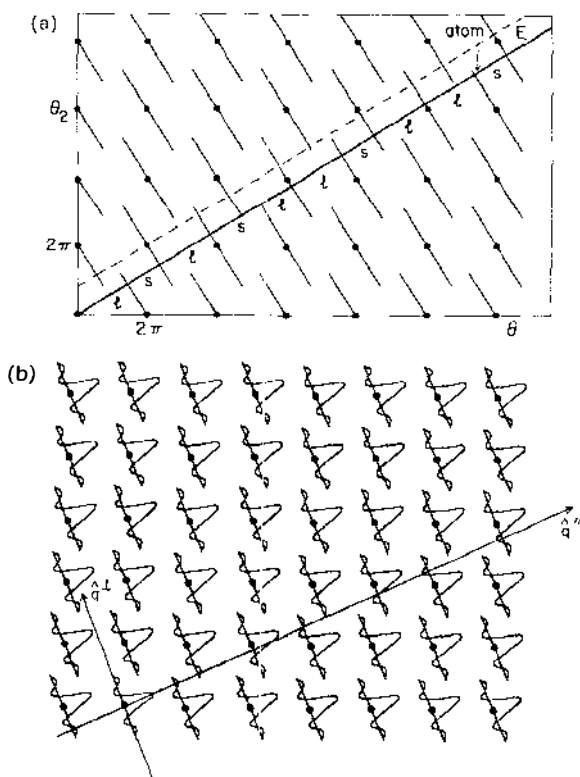


Figure 11 (a) Line segments represent atomic surfaces placed at sites of a two-dimensional square lattice. Intersections of atomic surfaces with one-dimensional physical space E place atoms in a Fibonacci sequence. (b) Fourier transform of Fibonacci sequence obtained from placing Fourier transform of atomic surfaces at sites of two-dimensional reciprocal lattice (after Ref. 67).

segments shown in Figure 11a yield the Fibonacci sequence along the physical space line E.

One of the greatest advantages of representing physical structures in hyperspace is the insight gained (48, 51–57) into the dependence of diffraction peak intensities and widths on \mathbf{G} and \mathbf{G}_\perp . To Fourier transform a quasiperiodic structure, first Fourier transform the atomic surfaces in the direction \mathbf{G}_\perp , then place copies of this Fourier transform at the sites of the reciprocal lattice in hyperspace, as shown in Figure 11b (52). The Fourier transform in physical reciprocal space \mathbf{G} consists of a delta function at every intersection of physical reciprocal space with the hyperspace diffraction pattern. The amplitude of the delta function in the physical reciprocal space equals the amplitude of the hyperspace diffraction pattern at the point of intersection. Clearly, this amplitude depends on \mathbf{G}_\perp and falls off for large values of \mathbf{G}_\perp . Because of the irrational slope of physical space within hyperspace, the diffraction peaks fill reciprocal space densely, but most of the peaks are quite weak because they have large amplitudes of \mathbf{G}_\perp .

A hypercubic crystal of atomic surfaces in six-dimensional space represents the microscopic, atomic structure of a quasiperiodic, icosahedrally symmetric material. Direct determination of the six-dimensional electron density of Al-Li-Cu exploits this observation (93, 134–136). Figure 12 shows the resulting Patterson functions in three hyperplanes. Inspecting Figure 11, one notices that the representation of atoms within the two-dimensional hyperspace is a set of line segments instead of points. The intersections of the one-dimensional physical space with the atomic surface is a set of points representing atomic positions. By analogy, in six dimensions the atomic surfaces must be represented by a set of three-dimensional volumes.

The central, pie shaped, region in Figure 12 represents a twofold symmetric plane in physical space. Contours indicate variation of electron density with position. The other two regions represent hyperspace planes, each one spanned by one hyperspace fivefold axis and one real space axis of (top region) fivefold symmetry or (bottom region) twofold symmetry. Basically, the electron density is high at the vertices of a hypercubic lattice and at the midpoints of edges. Presumably, these surfaces represent aluminum and copper. Body center surfaces may be occupied by lithium, which has low electron density (136) and, therefore, cannot be clearly resolved by x-ray scattering. The chemical structure of the atomic surfaces is not yet known precisely. Another remaining question is whether the atomic surfaces are faceted, smooth, or discontinuous. This issue is important because, as observed above, the shape of the atomic surface affects the placement of atoms in physical space. Achieving reasonable density and interatomic distances is a delicate matter. Furthermore, the topology of the atomic surfaces affects the dynamics of quasicrystals (137).

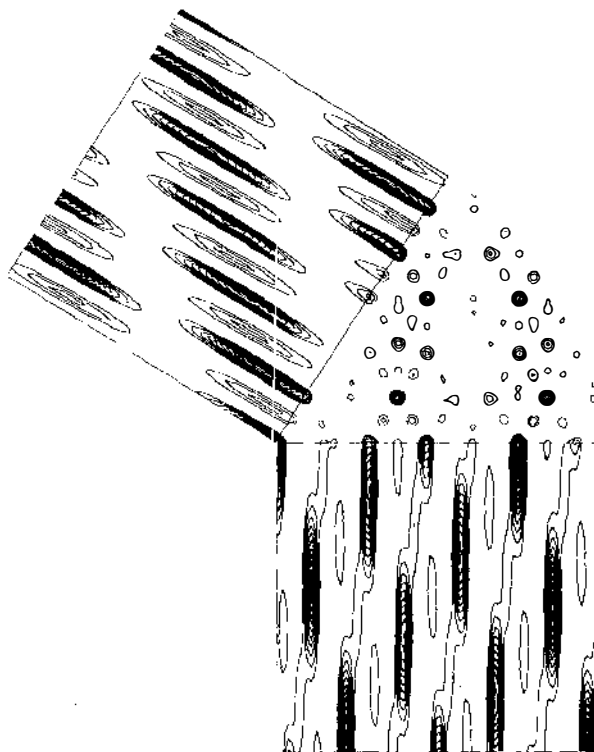


Figure 12 Patterson function in six dimensions obtained from x-ray data on Al-Li-Cu. Three views are shown, including a twofold symmetric plane in physical space and two planes that include the hyperspace fivefold axis and either a fivefold or twofold physical space axis. (Courtesy of M. V. Jaric.)

If the crystallographic analysis described above were performed with absolute precision, and there were no diffuse scattering present (which is not included in the analysis just described), then knowledge of atomic surfaces in six-dimensional space would completely determine the placement of each atom in real space. Unfortunately, one finds experimentally that the atomic surface occupation probabilities fall off smoothly, probably because of the neglect of infinitely many very weak peaks (138). It is then ambiguous whether there are fractional occupation probabilities and whether there is additional unresolved structure. In fact, the six-dimensional analysis suggests that the local structure in real space can be described by decorating rigid tiles with atoms or filling space with overlapping clusters, such as those illustrated in Figure 10*a*. The similarity to the simplest decorations of rhombohedral tiles is quite striking.

3.3 Phason Disorder and Approximants

So far, our six-dimensional space picture of the quasicrystal structure represents only a perfectly ordered quasiperiodic idealization. Elementary excitations, such as phonons, must enter at finite temperatures. Phonon modes represent displacements of atoms in the physical space; hence, they may be described as compressions and shears of the six-dimensional lattice parallel to the three physical dimensions. That leaves open the meaning of distortions in the perpendicular space. Inspection of Figure 1*a* suggests the following result. Displacements in the perpendicular space (*dashed line*) lead to the emergence of new intersections of atomic surfaces with physical space, and the loss of others nearby. Such disappearance, and nearby reappearance, of atoms leads to a localized structural rearrangement of the quasicrystal. These new excitations belong to a family of perpendicular space deformations. They generalize our concept of elementary excitations to include a family of discrete atomic jumps. In accordance with the terminology from ordinary incommensurate structures (139), these modes are termed “phasons” (51).

Localized phason fluctuations randomize the structure without altering the long-range order or lowering the rotational symmetry, just as thermal phonons leave intact ordinary crystalline order. But, long wavelength phason strain, created by a uniform shear of the six-dimensional structure, has a significant impact. Such strains reduce the rotational symmetry from icosahedral to cubic, rhombohedral, or lower. Carefully chosen shears lead to commensurate slopes between physical space and the hyperspace crystal, thus creating spatially periodic, crystalline (107, 140) structures. We call such structures “approximants,” because they exist in infinite families with ever smaller phason strain and converge towards the uniform strain free quasicrystal structure. Random inhomogeneous phason strain within a quasicrystalline structure (17, 58–60) broadens the peaks to a degree roughly linear in G_{\perp} . In contrast, uniform phason strain shifts peaks in a single crystal diffraction pattern, but broadens or splits peaks in a powder pattern.

Mechanisms, such as finite grain size broadening and strain broadening, affect diffraction patterns of ordinary crystals (141) in distinct ways. By denoting the average grain size by L , we obtain the half-widths of peaks in the diffraction pattern $\Delta Q = \sqrt{(\pi/L)^2 + (\Delta Q_{\text{res}})^2}$, where ΔQ_{res} is the instrumental resolution. The broadening is independent of the wavevector of the diffraction peak, although peaks of different symmetries can broaden to different degrees by this mechanism because of anisotropic grain shapes. In contrast, inhomogeneous strains in a crystal broaden by an amount ΔQ which is proportional to G .

The diffraction peak broadening observed for simple icosahedral alloys

follows neither trend. Instead, ΔQ increases almost linearly with G_{\perp} (17) (see Figure 13a). This implies the dominant strain mechanism in SI alloys originates in the phason-like, rather than phonon-like, degrees of freedom. Furthermore, this “phason-strain” mechanism appears universal among SI alloys because slowly cooled stable alloys of Al-Li-Cu (142) share the same systematics, and nearly the same magnitude, of broadening with rapidly quenched metastable alloys Al-Mn (17). Interestingly none of the FCI alloy diffraction peaks broaden with these systematics. Figure 13b shows that in the FCI Al-Cu-Ru alloy, the peak widths increase linearly with G_{\parallel} , rather than G_{\perp} (47). Therefore, normal lattice strain dominates phason strain as a mode of disorder. High-resolution single grain diffraction measurements of Al-Cu-Fe find no line broadening above instrumental resolution, thus corresponding to positional coherence lengths in excess of 8000 Å (45).

Discriminating between the diffraction patterns from true quasicrystals and large unit cell periodic approximants can be quite difficult. As the size of the unit cell increases (and/or the symmetry of the unit cell decreases) the density of Bragg points in reciprocal space also increases. The internal arrangement of atoms within each unit cell largely determines the intensities of diffraction peaks, so selected area electron diffraction patterns from large unit cell approximant phases are barely distinguishable from their quasicrystalline cousins. Even CBED patterns may fail to distinguish between quasicrystalline and large unit cell approximant structures because, as pointed out by Levine et al (143), Kikuchi bands in CBED patterns reflect the symmetry of the dominant scattering cluster of atoms in the phase. For small unit cells, the dominant clusters are the unit cells themselves. For large unit cell approximants, the icosahedrally symmetric atomic basis within the unit cells dominates the scattering.

Quite often, one or several approximant phases coexist with the quasicrystalline structure in the same alloy, generally with a coherent orientational relationship between adjacent grains of the icosahedral and crystalline phases (144, 145). Some of the axial approximant phases have already been mentioned in Section 2.2. Particularly striking examples of approximants to icosahedral structures (129, 130) appear in the Ga-Mg-Zn system. Figure 14 shows the electron diffraction patterns taken along the “pseudo” fivefold axes of three of the six known approximant phases, along with the fivefold axis of the true icosahedral phase. Although the diffraction patterns from these approximant phases are distinguishable from that of the icosahedral phase, the pattern of the most intense spots clearly indicate the internal icosahedral symmetry of the atomic basis in the crystalline unit cells.

In some cases the selected area diffraction patterns of crystalline approximants are very difficult to distinguish from those of an icosahedral alloy

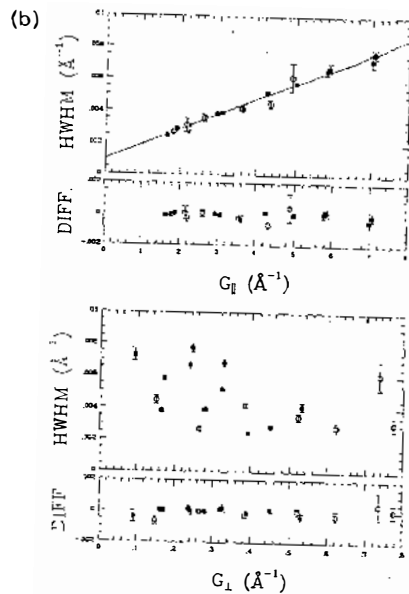
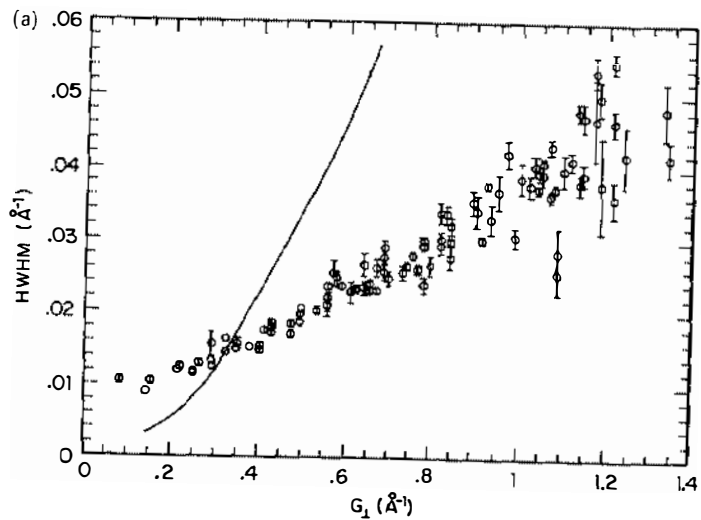


Figure 13 (a) Diffraction peak broadening as a function of phason momentum in simple icosahedral Al-Li-Cu (courtesy of C. Guryan). The line represents widths predicted by P. W. Stephens in Ref. 162. (b) Diffraction peak widths as a function of phason momentum in FCI Al-Cu-Ru [after Ref. (47)]. The filled (*open*) circles denote peaks of all even (*odd*) indices.

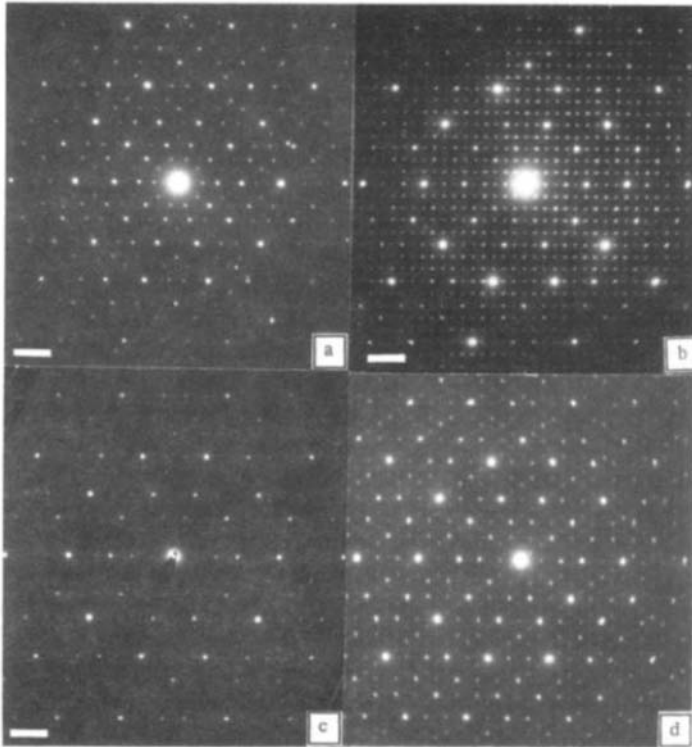


Figure 14 Fivefold and pseudo fivefold diffraction patterns of the icosahedral phase and three approximants in the Ga-Mg-Zn system: (a) $\tau/1$ ideal icosahedral, (b) $3/2-2/1-2/1$ type side centered orthorhombic phase [110] zone axis, (c) $2/1$ cubic phase; [058] zone axis, (d) $2/1$ rhombohedral phase; [001] zone axis. The marker corresponds to 1 \AA^{-1} . (Courtesy of F. Spaepen.)

with significant anisotropic linear phason strain because, to first order, both yield subtle peak shifts or anisotropy in the diffraction pattern. High-resolution single grain x-ray diffraction measurements distinguish the approximant phase from true icosahedral phase by characteristic splitting or asymmetric broadening of diffraction peaks (P. W. Stephens, P. A. Bancel, private communication). In powder diffraction measurements, however, the directional averaging all but obscures distinct peak splitting. Because the diffraction peaks from the approximant phase are closely spaced, powder measurements show only an apparent broadening of the diffraction peak lineshapes, which scales with G_{\perp} (146).

4. STRUCTURAL PARADIGMS

We now distinguish between several paradigms of quasicrystal structure. Some models explicitly describe nonequilibrium, disordered structures.

These models come under the general heading of “icosahedral glass,” and, so far, appear most relevant to SI quasicrystals. Other models describe thermodynamically stable phases with perfect, long-range quasiperiodic positional order. These include Penrose tiling models and their generalizations and random tiling models. Before examining novel quasicrystal structures, one must first address whether quasicrystals are ordinary crystalline materials that generate a false appearance of icosahedral symmetry of twinning.

4.1 *Twinning*

Multiple twinning during metallic crystal growth is well known and commonly observed. Pseudoicosahedral or pseudodecagonal symmetries in multiply twinned structures arise when the relative orientations of twin variants obey icosahedral or decagonal point group symmetries. In their analysis of the electron diffraction patterns of rapidly quenched Al-Mn, Field & Fraser (147) concluded that the diffraction patterns likely arose from microtwinning among 20 twin variants of a distorted diamond cubic lattice. A similar mechanism explains the formation of icosahedral clusters of gold from the vapor. Other microtwinning models (148), based on rhombohedral distortions of small FCC crystals (149, 150), have been proposed to describe the structure of the icosahedral phase. Although these models reproduce many features found in the diffraction patterns of Al-Mn, significant multiple scattering contributions prove necessary to reproduce the diffraction patterns in detail.

The twinning hypotheses can be tested in several ways (151). Selected area diffraction utilizes a large beam aperture ($\approx 1 \mu\text{m}$) and, therefore, cannot clearly distinguish between true icosahedral symmetry and a set of small icosahedrally twinned periodic crystals. On the other hand, CBED focuses the electron beam down to sizes on the order of 20–100 Å, thus revealing the symmetry of the Kikuchi bands and higher order Laue zones (HOLZ) in the diffraction pattern. For reasonably small unit cells (on the order of what one typically finds for metals), the symmetry of the unit cell should be evident in both the Kikuchi bands and the HOLZ lines. Dark field imaging, in which one selects a subset of diffraction peaks to produce an image of the sample, determines which portions of a particular grain contribute to the intensity of selected diffraction spots. Indeed, this technique revealed the occurrence of fivefold twins of the orthorhombic Al_6Mn crystalline phase and distinguished them from the dark field images produced by the icosahedral phase of Al-Mn (D. Shechtman, unpublished data). Finally, HREM images produced by “retransforming” the electron diffraction pattern may be examined for evidence of these microtwins. All of these tests, applied to electron diffraction patterns from icosahedral alloys, provide little support for the small unit cell microtwinning models.

X-ray diffraction experiments rigorously test the validity of those twinning models that require multiple scattering for agreement with experimental diffraction patterns. Multiple scattering affects x-ray diffraction much less severely than electron diffraction, because electrons interact more weakly with photons than with other electrons. Observation of higher-order diffraction peaks in high-resolution x-ray powder measurements on the Al-Mn icosahedral alloy (50) excludes any twinning model that requires strong multiple scattering to explain the diffraction pattern. Furthermore, single grain x-ray precession photographs that use monochromatic radiation yield diffraction patterns in substantial agreement with the corresponding electron diffraction patterns (152).

The various moderate-size unit cell cubic crystal/twinning models, proposed by Pauling (153), may also be tested by precise x-ray measurements of diffraction peak positions. Because the ratio of the d-spacing of any two collinear diffraction peaks from a periodic crystal must be the ratio of two integers, careful measurements of diffraction peak positions set limits on the minimum size of the cubic unit cell required to produce that sequence of diffraction peaks. For the Al-Mn alloy, the two lowest angle diffraction spots observed along a twofold direction correspond to d-spacings of $8.85 \pm 0.07 \text{ \AA}$ and $5.42 \pm 0.03 \text{ \AA}$, respectively. The simplest rational approximation to the ratio 1.63 ± 0.02 of these d-spacings, within experimental error, is $13/8 = 1.625$. Therefore, the minimum size cubic cell is on the order of $8 \times 8.85 \text{ \AA} \approx 70 \text{ \AA}$. The 26.7 \AA and 23.4 \AA cubic unit cells proposed by Pauling for this structure cannot produce collinear spots with the observed spacings, even assuming multiple twinning (154). The FCI icosahedral alloy Al-Cu-Fe constrains the minimum unit cell size even more strongly, as diffraction peak broadening, the main contribution to uncertainty in the determination of diffraction peak positions, is all but absent here. Bancel's (45) single grain x-ray diffraction data requires a unit cell size greater than 185 \AA (155) in any cubic twinning crystal twinning model, thus ruling out Pauling's (156) proposed 52 \AA unit cell structure. Furthermore, all of the cubic twinning models require significant multiple scattering to obtain the complete set of the diffraction spots observed in both the electron and x-ray diffraction.

Despite the inadequacy of these particular twinning models in explaining diffraction data of the icosahedral phase, there is a sense in which the models are on the right track. Namely, even well-ordered, equilibrium FCI (45) and decagonal (151) quasicrystals apparently crystallize as temperature drops (however, it is not yet certain whether this transition occurs in *all* equilibrium quasicrystal-forming compounds). But at these low temperatures, growth of the bulk crystal is kinetically limited. As a result, the structure consists of myriad microscopic crystallites, each only a few

unit cells in size, which are oriented so that overall icosahedral symmetry is preserved (126). The x-ray powder diffraction pattern of this state differs from the diffraction pattern of the quasicrystal phase only by a slight broadening of peaks, which scales with G_{\perp} (158), although HREM reveals its true twinned microcrystalline state.

4.2 Icosahedral Glass

The leading model of nonequilibrium quasicrystals is known as the icosahedral glass model (1, 159). In this model (Figure 15a), atomic clusters, such as those illustrated in Figure 10a, join in a manner that preserves

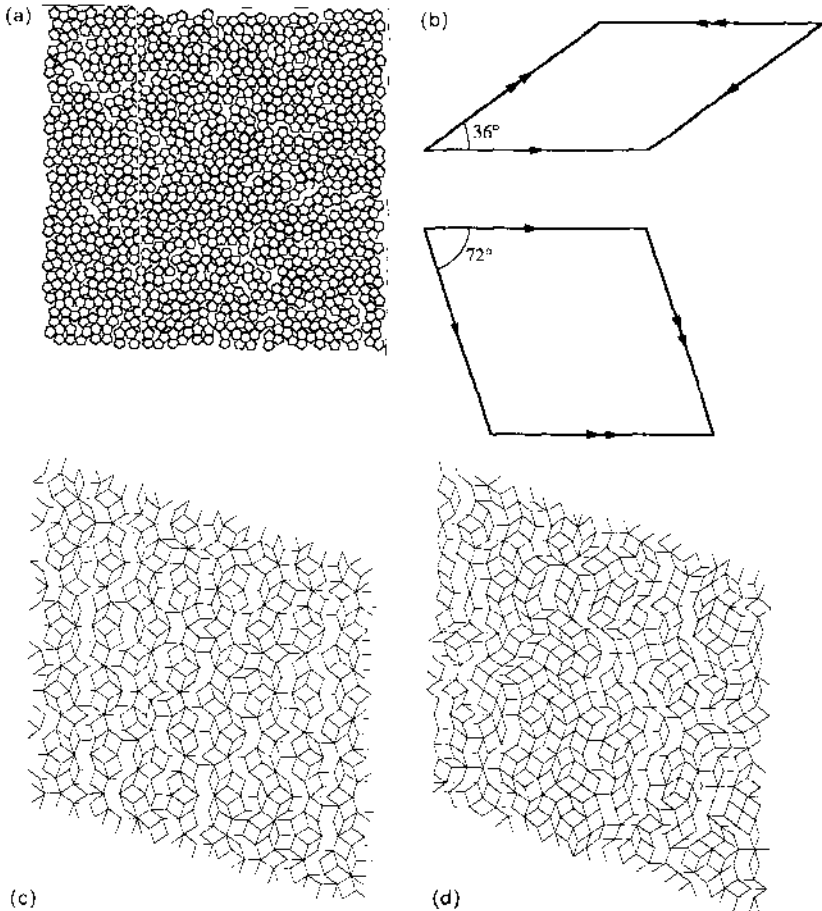


Figure 15 (a) Glassy aggregate of pentagons. (b) Penrose rhombia illustrating matching rules. (c) Penrose tiling by rhombi with matching rules. (d) Random tiling without matching rules.

icosahedral orientation, but need not preserve long-range positional order. In fact, rapid growth of such structures creates “tears”—surfaces within the glass along which positional order breaks down. Slower growth (160, 161) avoids tears, but incorporates uniform phason strains in regions of the sample related to the direction of growth. In terms of the six-dimensional description of quasicrystalline structures, the icosahedral glass corresponds to a cut through a hyperspace crystal with abrupt, random shears along the perpendicular space direction. These shears introduce tears in the real space structure, along which chemical bonds are broken. The disorder broadens diffraction peaks by an amount dependent on G_{\perp} .

Let \mathbf{h}_{\perp} measure the perpendicular space displacement of the hyperspace crystal. The diffraction peak widths depend on how \mathbf{h}_{\perp} varies with position in the sample. For example, if $\mathbf{h}_{\perp} = 0$, the real space structure is an ideal quasicrystal with delta function Bragg peaks. On the other hand, if \mathbf{h}_{\perp} executes a random walk, then $\langle |\mathbf{h}_{\perp}|^2 \rangle \sim |\mathbf{r}|$, and the diffraction peak widths grow like G_{\perp}^2 . If, instead, $\langle |\mathbf{h}_{\perp}|^2 \rangle$ increases as $|\mathbf{r}|^2$, the diffraction peak widths grow only as $|G_{\perp}|$. Early simulations of aggregation attach icosahedra at their faces in a manner that preserves bond orientational order and forbids overlap of neighboring icosahedra. Such algorithms produced many tears and caused \mathbf{h}_{\perp} to execute a random walk. Peak widths in these simulations grow as G_{\perp}^2 or faster (162). Experimentally, it seems that SI alloy peak widths grow only linearly with G_{\perp} .

Robertson & Moss (163) modified the rules for growing the icosahedral glass in a manner that increases the density, decreases the number of tears, and produces diffraction peak widths linear in G_{\perp} . Furthermore, the magnitude of the diffraction peak widths obtained from their simulations are in closer agreement with those found for the SI alloys. There are two key ingredients of their algorithm:

1. Restrict local attachments to include only those that produce second neighbor cluster configurations found in cubic α -Al-Mn-Si alloy or in a perfect quasicrystalline packing (three-dimensional Penrose tiling) of clusters. This constraint discriminates against local configurations that produce large voids in the network.
2. Grow the structure in concentric shells of a small thickness (roughly 0.2 cluster diameters) and require that each shell be filled before starting the next shell.

Elser and coworkers (160, 161) developed a dynamic growth algorithm for the icosahedral phase based upon formation and aggregation of icosahedral clusters at the solid-liquid interface. In addition to the essential constraints regarding bond-orientational order and overlap of the “static” algorithms described above, clusters may adjust their positions at the

growth interface to maximize the connectivity and density of the structure. This step reduces the density of tears, or gaps, in the icosahedral glass network, which results in diffraction peak widths that scale like G_{\perp} in agreement with experiments.

4.3 *Equilibrium Models*

Well-ordered quasicrystal models stand in contrast to twinning and icosahedral glass models, because they describe structures with infinite positional correlation lengths in thermodynamic equilibrium. Two principal models of this class, one based on Penrose tilings, the other on random tilings, resemble one another superficially, but differ in their explanation of the origin of quasiperiodicity. Both models fill space with rigid tiles. Figure 15c illustrates the Penrose tiling by filling the plane with 36° and 72° rhombi. Penrose tilings obey “matching rules,” which guarantee quasiperiodicity. The matching rules require matching up the arrows shown in Figure 15b on every common edge of rhombi in a tiling. Except for shifts of origin, the resulting structure is unique.

Steinhardt and coworkers (164, 165) proposed Penrose tilings and their generalizations as models for quasicrystalline materials. These models enjoy great success because of their qualitative agreement with diffraction patterns of real quasicrystalline materials. Penrose tilings possess many remarkable geometrical properties related to their quasiperiodicity (166, 167). For instance, a particular subdivision of the tiles, known as a “deflation,” creates a new identical tiling with edge lengths scaled down by a factor of τ . This is related to the ambiguity in the scaling of diffraction patterns by τ or τ^3 .

Certain difficulties remain in this class of models, however. Most notably, these concern the reliance on matching rules to force quasiperiodic order, and whether structures obeying these rules can ever grow. This latter question arises because there is no truly local set of rules for growing Penrose tilings from a central point (168). The matching rules illustrated in Figure 15b, for example, guarantee that a tiling is Penrose if it obeys the rules at all points in space. But, adding tiles in a manner consistent with all the geometrical properties of Penrose tilings requires a nonlocal search of the tiling perimeter. Failure to conduct such a search introduces phason strain through violations of the matching rules. The flaw may not be fatal, however, because enhancements to the matching rules (169, 170) allow growth at slow rates with extremely low density of matching rule violations. Inclusion of a single topological defect (analogous to a screw dislocation) in the seed aids rapid growth.

Onoda et al (169) have suggested that energetic interactions among atoms conspire, not only to create geometrical tiles, such as those in Figure

10*b-d*, but also to create interactions between these tiles that mimic matching rules. In such a system, a quasiperiodic structure forms the ground state at absolute zero. Unfortunately, delicate balancing of atomic pair potentials at large distances may be required to ensure that any particular quasiperiodic structure is a ground state (171). This is because localized phason fluctuations, which correspond to rearrangement of a small number of atoms, often leave the pair correlation function unaltered out to large distances. Requiring that the resulting small changes in energy be positive places constraints on the potentials at the corresponding length scale. Accordingly, no continuum atomic model has yet been proposed for real or hypothetical quasicrystals that reproduces the Penrose tiling structure.

In fact, matching rules are not needed to explain quasiperiodic long-range order. Many hypothetical (172–175) and realistic (8, 63, 64, 124, 126, 176) models explain the occurrence of fundamental clusters or decorated tiles on the basis of atomic interactions, but find near degeneracy for differing arrangements of the basic building blocks in space (provided obvious constraints are obeyed). That is, the energy for arranging the tiles in a Penrose-like structure agrees roughly with the energy for arranging the tiles into large unit cell approximants, or many other structures. This near degeneracy suggests consideration of tiling entropy (114, 177, 178) and its influence on long-range structure. One finds that among all conceivable tilings, the one with highest entropy (i.e. the most probable) shares the long-range quasiperiodicity of the Penrose tiling (179–181). That is, random tilings differ from Penrose tilings because of great numbers of localized phason fluctuations, but share the central characteristic of quasiperiodic long-range order.

Thermodynamic stability of the quasicrystal state in random tiling models depends on the same configurational entropy that creates quasiperiodicity. The degeneracy of random tiling models will not be perfect in reality. Energetic interactions among tiles presumably cause a phase transition into an ordinary crystal state at low temperatures. As temperature rises, entropy of random tilings dominates energetic preference for the crystal state, thus leading to a phase transition (96, 182–184) into an “entropically stabilized” quasicrystal state. Experimentally, such phase transitions apparently do occur in some FCI and other equilibrium quasicrystal-forming compounds (45, 126, 157). For instance, in $\text{Al}_{65}\text{Cu}_{23}\text{Fe}_{12}$ the state is crystalline at temperatures below 670°C with an apparent rhombohedral unit cell size of 37.7 Å and angle $\alpha = 64.43^\circ$. Above 670°C, the state is quasicrystalline, and diffraction peaks sensitive to phason fluctuations (those with large $|\vec{r}_\perp|$) appear to grow in intensity as temperature increases (45). Theoretically, entropic stabilization predicts such

a growth in intensity because the phason elastic constants increase with temperature (182, 183). Explaining quantitatively the instability of the quasicrystal phase and the transition (which appears weakly first order) into a crystal phase at low temperatures remains an open problem (80, 81, 140, 157, 184–187).

Although tiling models enjoy many qualitative successes, describe quasicrystal structure and explain the origin of quasiperiodicity, they are not capable of predicting new quasicrystalline compounds. Energetic preferences for icosahedral clusters and other geometrical and chemical assumptions are made implicitly to restrict attention to geometrical clusters. The properties and interactions of real atoms are ignored. A phenomenological theory based on quantum structural diagrams (188–191) finds that compounds favor icosahedral order only over limited ranges of composition-weighted electronegativity. Marginal crystalline-compound-forming ability appears to be an additional requirement. On this basis, several metastable quasicrystal-forming compounds were proposed, including Ga-Mg-Zn, Ag-Mg-Al, Zn-Li-Al, and Au-Li-Al in proportions of 15 : 35 : 50, which have been experimentally confirmed (189–191). Providing a scientific basis for such a phenomenological theory requires examination of electron band structure.

5. MATERIALS PROPERTIES

5.1 *Electronic and Vibrational Band Structure*

Quasicrystals may show unusual electronic and vibrational properties that result from their quasiperiodic order and icosahedral symmetry. In nearly free electron models, electron dispersion relations follow the free electron parabola, except near Brillouin zone boundaries, at which point avoided level crossings open gaps (46). Materials in low dimensions show such effects most clearly. In one dimension, avoided crossings create gaps in the density of states (DOS). In two or more dimensions, gaps need not appear in the DOS because the zone boundary position depends on direction in reciprocal space. Still, zone boundaries create DOS singularities that diminish in strength as dimension increases.

Fibonacci sequences provide a one-dimensional laboratory for examining the effects of quasiperiodicity (192, 193). The quasiperiodic structure fills reciprocal space densely with Bragg peaks. At a wavevector equal to half the magnitude of the wave vector of each peak, a gap opens in the band structure (Figure 16) so that the dispersion relation acquires a dense set of discontinuities. Alternatively, we describe the band structure by considering a series of periodic approximants to the quasiperiodic Fibonacci sequence. For each approximant, the band structure contains a num-

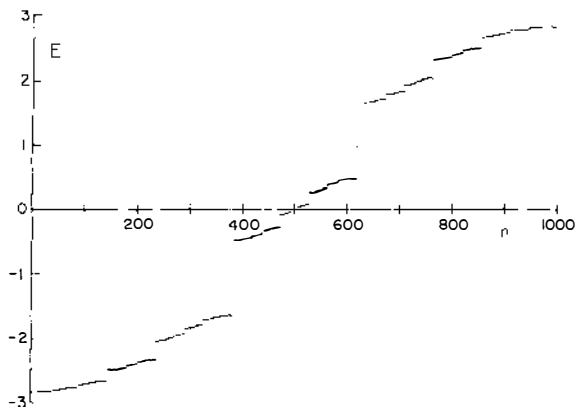


Figure 16 Band structure of Fibonacci chain. The horizontal axis plots mode number (in a periodic lattice, this would be wave number); energies are plotted vertically. (Courtesy of F. Nori.)

ber of bands equal to the number of sites in the approximant unit cell. As this unit cell size grows, each band splits up into a collection of smaller bands, each collection mirroring the entire band structure of the previous approximant. In the limit of infinite cell size, the band structure becomes a Cantor set. Intermediate between the continuous bands of a crystalline chain and the pure point spectrum of a random chain, such a band structure is called “singular continuous” (194).

Continuous electron bands with extended electronic eigenstates allow electrical conductivity (46). Point spectra with exponentially localized eigenstates prevent conductivity (195). A Cantor set spectrum is an interesting intermediate case. The electronic states decay algebraically according to a self-similar function (they are “critical”). It is natural to wonder whether a material with such a band structure will be an insulator or a conductor. When the Fermi energy lies on an allowed level, the transmission coefficients depend on the locations of the edges of the sample and on the phase of the wavefunction (196). Even when the Fermi energy lies in one of the gaps, the exponential decay of the wavefunction may be so slow that in a system of finite size the conductivity is appreciable (194).

In higher dimensions singularities, but not in general gaps, appear in the DOS. In fact, Sokoloff (197) has shown that in three dimensions, a perfect quasilattice, such as a Penrose lattice, conducts electrons without resistivity. Actual resistivities tend to be quite high in real quasicrystalline materials, which range from $150 \mu\Omega\text{-cm}$ in U-Pd-Si (16) to $5000 \mu\Omega\text{-cm}$ in Al-Cu-Ru (198). This latter value lies close to the minimum metallic conductivity (199). The high resistivities are partly due to a low electronic

density of states at the Fermi surface. Measurements (200) and calculations (201, 202) reveal that the Fermi surface lies in a pseudogap for both the quasicrystal and its approximants. Yet, the resistivity of the quasicrystal state exceeds that of the crystal approximant by as much as a factor of six. This may reflect the "critical" nature of wavefunctions near the Fermi energy (201, 202). Or, a combination of intrinsic disorder, perhaps similar to random tiling disorder, and resonant d-band scattering creates unusually short electron mean free paths (197).

Total energy calculations and "Hume-Rothery" considerations may help explain stability of quasicrystal forming compounds. Total energy calculations of clusters of d-band atoms by Phillips & Carlsson (203) find the energetic preference for icosahedral structure extends only over a range of roughly 2–5 d-band electrons per atom. Furthermore, they suggest that electronic stability of tetrahedrally close packed crystals (124) and quasicrystals requires an angle-dependent, four-body interaction. Band structure calculations of quasicrystalline and related crystalline structures (201, 202, 204–207) reveal densities of states containing Van Hove singularities and pseudogaps. When the Fermi energy lies in a DOS minimum (i.e. a diffraction peak lies at $Q = 2k_F$) quasicrystal formation is favored (208). Experimental studies (200) of trends in Hall coefficients, thermopowers, and low temperature specific heats as composition is varied reveal the presence of pseudogaps and support the notion of Hume-Rothery stabilization for electron ratios close to 2.17 and 2.42 electrons/atom.

Neutron scattering measurements of the vibrational density of states (VDOS) of Al-Mn (209) and U-Pd-Si (210) icosahedral alloys show considerably less structure than corresponding crystalline phases close by in composition. In fact, the frequency spectrum of icosahedral U-Pd-Si resembles that of the glassy phase. Based upon theoretical and experimental studies of one- and two-dimensional quasiperiodic systems (193, 211–215) one might expect a great deal of structure in the VDOS of quasiperiodic alloys. The absence of sharp structure may result from orientational averaging intrinsic to powder measurements, the effects of finite instrumental resolution, or decreasing strength of singularities in high dimensions. The similarity between the icosahedral and glassy VDOS in Al-Mn and U-Pd-Si suggests that short-range order in the quasicrystal phase resembles that of the glassy phase.

In contrast, the VDOS of icosahedral Al-Li-Cu resembles the VDOS of the cubic R-phase. Both show distinct bands at nearly the same frequency with variances only in the relative weight of the peaks (216). This result suggests similar short-range order and interatomic forces in both the icosahedral phase and its cubic approximant. Low temperature acoustic measurements of atomic tunneling states in Al-Li-Cu and Al-Mg-Zn like-

wise show that the extent of disorder in the icosahedral phase is appreciably closer to the crystalline, rather than glassy, phase. Interestingly, this measurement also correlated the density of tunneling states with the degree of phason strain (217).

Single grain inelastic neutron scattering measurements on Al-Li-Cu (218) and Al-Cu-Fe (219) icosahedral phase alloys show that the low-lying acoustic branches of the dispersion curves are isotropic. This isotropy is expected because of the high symmetry of the icosahedral point group (8) and is also observed in ultrasonic measurements on single grains of Al-Li-Cu (220). In Al-Li-Cu, the acoustic branches well away from the zone center exhibit “quasi”-zone boundaries. Furthermore, the phonon spectrum of longitudinal modes along icosahedral twofold axes resembles theoretical calculations for a one-dimensional Fibonacci chain (221–224). This may be because the sequence of strong diffraction peaks along the twofold axis resembles that from a Fibonacci sequence.

5.2 Magnetism

Splitting of atomic orbitals depends sensitively on the local symmetry of the crystal field at individual atomic sites. Cluster models of quasicrystals suggest the presence of sites with nearly icosahedral symmetry—a symmetry sufficiently high that atomic d-bands remain unsplit. In contrast, cubic or lower symmetry splits the band into two or more components. As a result, a substantial d-band DOS close to the Fermi energy may be localized on these sites. This could (225, 226) enhance the tendency towards magnetism, encourage vacancy formation, or cause distortions of the local symmetry (201, 202).

The crystalline phases cubic α -Al-Mn-Si, orthorhombic Al_6Mn , and β - Al_4Mn do not exhibit magnetic moments, whereas the icosahedral phases of Al-Mn and Al-Mn-Si, at Mn concentrations higher than 14 atomic %, exhibit magnetic moments that increase with increasing Mn concentration (227–229). A simple model explains the concentration dependence of the moment (230) by postulating two classes of sites: one magnetic, one nonmagnetic. This scheme first populates the nonmagnetic sites, then fills the additional magnetic sites after the Mn concentration exceeds 14 atomic %. Studies of Cr and Fe substitutions for Mn (231–233) support this picture. Substitution of Fe for Mn affects the magnetic moment only slightly (presumably because it sits on the nonmagnetic sites), whereas replacement of Mn by Cr decreases the moment in proportion to the decrease in the Mn concentration. NMR and Mossbauer measurements of Al-Mn alloys and Al-Cu-Fe, however, question the validity of this two-site model. Instead they suggest a continuous distribution of transition metal sites (234–236). Interestingly, icosahedral Al-Cu-Fe is weakly dia-

magnetic with a temperature independent susceptibility. The magnetic moment in the icosahedral phase may not be intrinsic, but instead may arise from small clusters of Mn (231–233, 237). The origin of a magnetic moment in the icosahedral alloys, still the subject of controversy, has been reviewed by Stadnik et al (236).

Both Al-TM and U-Pd-Si icosahedral alloys exhibit Curie-Weiss susceptibility with negative Θ , which indicates antiferromagnetic exchange interactions between magnetic ions. At low temperature, cusps in the ac susceptibility for these alloys are observed. Several groups (227, 238, 239) report a transition to a spin-glass state in Al-Mn. In U-Pd-Si, the absence of a difference in field cooled and zero-field cooled ac susceptibility suggests an antiferromagnetic transition (240).

Although Al-TM-Si quasicrystals with low metalloid concentrations choose paramagnetic or spin-glass ground states, higher metalloid (Si or Ge) concentrations favor ferromagnetism. Ferromagnetism occurs in both glassy (227) and icosahedral (241) Al-Mn-Si alloys for Si concentrations in excess of 25–30 atomic % with $T_C \approx 100$ K. Ferromagnetism was also reported in samples of icosahedral Al-Mn-Ge ($T_C \approx 530$ K) and Al-Cu-Mn-Ge ($T_C \approx 470$ K) for Ge concentrations in the range of 20–30 atomic % (242). Measurements of the temperature dependence of the magnetization in a magnetic field of 4 kOe however, reveal an oddly shaped (concave, rather than convex) order parameter, which suggests that the order is not quite ferromagnetic. Very recent studies indicate that the apparent magnetic ordering in these samples arises from small inclusions of a second phase of crystalline AlGeMn (Fe) (243).

CONCLUSIONS

In summary, we remind the reader of the principal characteristics of quasicrystals described in this paper. Thermodynamically stable quasicrystal states possess icosahedral and decagonal symmetry. Because icosahedral and decagonal symmetry are crystallographically forbidden, their translational order is quasiperiodic, rather than periodic. Six-dimensional spaces therefore prove useful for both indexing the diffraction patterns and describing the real-space atomic structure. In addition to the quasiperiodic spatial order, quasicrystals differ from ordinary crystals, as they possess a class of fluctuations known as “phasons,” which corresponds to special types of atomic rearrangements. Uniform phason strain may cause a quasicrystal to crystallize, whereas phason fluctuations may play a role in stabilizing the quasicrystal state at high temperatures. Investigations of electronic properties of quasicrystals suggest that “Hume-Rothery” con-

siderations of pseudo-gaps in the electron band structure at the Fermi surface may also help explain quasicrystal stability.

Much remains to be studied in quasicrystal science. For example, one might ask whether icosahedral quasicrystals occur in Borates, Clathrates, or chiral liquid crystals (244). To date, only metallic quasicrystals are known, but there is no explanation for why nonmetallic materials should not possess such phases. Regarding the determination of quasicrystalline structure, the chief remaining problem appears to involve interpretation of regions of low occupation probability on the six-dimensional atomic surfaces. Are these regions the result of insufficient experimental resolution, or do they signify the presence of phason disorder? Aside from questions of this type, the structure problem appears essentially solved. One unsolved problem related to structure is the description of phason fluctuations at the atomic level and an explanation for their apparent mobility in FCI materials, but not in SI materials.

Of more pressing importance than these questions of existence and structure, however, are the related issues of materials properties and potential applications. Now that high quality samples are available, we hope that experiments can probe the intrinsic properties of quasicrystals. The macroscopic icosahedral symmetry and long-range quasiperiodic order may both lead to novel properties. The rotational symmetry alone, for instance, alters the form of macroscopic crystal tensors. The quasiperiodic translational order is expected to cause some electronic wave functions to become "critical." It would be of great interest to confirm this experimentally and to understand the impact of criticality on transport phenomena. Finally, one must ask whether the novel rotational and translational order of quasicrystals allows practical applications. A small number of potential applications have emerged, including the decorative uses of quasiperiodic patterns and a suggestion that quasicrystals be used as low-friction coatings on aluminum frying pans (245).

ACKNOWLEDGMENT

We wish to thank S. Ebalard, F. W. Gayle, K. Hiraga, L. X. He, M. V. Jaric, K. F. Kelton, A. R. Kortan, F. Nori, M. Shin, F. J. Spaepen, and K. J. Strandburg for providing figures used in this paper. We would like to thank H. F. Franzen, B. N. Harmon, and J. E. Shield for critical reading and comments on the manuscript. We acknowledge useful discussions with C. Guryan, C. L. Henley, R. W. McCallum, K. Rabe, and P. W. Stephens. Ames Laboratory is operated for the United States Department of Energy by Iowa State University under Contract No. W-7405-ENG. M. Widom

acknowledges support from the National Science Foundation through Grant No. DMR-8918810 and from the A. P. Sloan Foundation.

Literature Cited

1. Shechtman, D., Blech, I. 1985. *Metall. Trans. A* 16: 1005
2. Shechtman, D., Blech, I., Gratias, D., Cahn, J. W. 1984. *Phys. Rev. Lett.* 53: 1951
3. Jaric, M. V., ed. 1988. *Introduction to Quasicrystals*, Vol. 1. Boston: Academic
4. Jaric, M. V., ed. 1988. *Introduction to the Mathematics of Quasicrystals*, Vol. 2. Boston: Academic
5. Jaric, M. V., Gratias, D., eds. 1989. *Extended Icosahedral Structures*, Vol. 3. Boston: Academic
6. Strandburg, K., ed. 1991. *Bond Orientational Order in Condensed Matter Systems*. Berlin: Springer
7. Steinhardt, P. J., DiVincenzo, D. P. 1991. *Quasicrystals: The State of the Art*. Singapore: World Scientific
8. Henley, C. L. 1987. *Comm. Condens. Matter* 13: 59
9. Steinhardt, P. J., Ostlund, S., eds. 1987. *The Physics of Quasicrystals*. Singapore: World Scientific
10. Yacamán, M. J., Romeu, D., Castano, V., Gomez, A., eds. 1990. *Quasicrystals and Incommensurate Structures in Condensed Matter*. Singapore: World Scientific
11. Jaric, M. V., Lundqvist, S., eds. 1990. *Quasicrystals*. Singapore: World Scientific
12. Fujiwara, T., Ogawa, T., eds. 1990. *Quasicrystals*. Berlin: Springer-Verlag
13. Kuo, K. H., ed. 1987. Proc. Int. Workshop Quasicrystals, Beijing, China. *Mater. Sci. Forum* 22-24
14. Gratias, D., Michael, L., eds. 1986. *International Workshop on Aperiodic Crystals. J. Phys. Colloq.* 47: C3
15. Bancel, P., Heiney, P. A. 1986. See Ref. 14, p. 341
16. Poon, S. J., Drehman, A. J., Lawless, K. R. 1985. *Phys. Rev. Lett.* 55: 2324
17. Horn, P. M., Malzfeldt, W., DiVincenzo, D. P., Toner, J., Gambino, R. 1986. *Phys. Rev. Lett.* 57: 1444
18. Follstaedt, D. M., Knapp, J. A. 1987. *Nucl. Inst. Methods Phys. Res.* B24/25: 542, and references therein
19. Kimura, K., Hashimoto, T., Suzuki, K., Nagayama, K., Ino, H. 1985. *J. Phys. Soc. Jpn.* 54: 3217
20. Bendersky, L., Kaufman, M. 1986. *Philos. Mag. B* 53: L75
21. Chen, C. H., Chen, H. S. 1986. *Phys. Rev. B* 33: 2814
22. Ramachandrarao, P., Sastry, G. V. S. 1985. *Pramana* 25: L225
23. Mukhopadhyay, N. K., Subbanna, G. N., Ranganathan, S., Chattopadhyay, K. 1985. *Scr. Metall.* 20: 525
24. Ball, M. D., Lloyd, D. J. 1985. *Scr. Metall.* 19: 1065
25. Sainfort, P., Dubost, B., Dubus, A. 1985. *C. R. Acad. Sci. Paris* 301: 689
26. Tsai, A., Inoue, A., Masumoto, T. 1988. *J. Mater. Sci. Lett.* 7: 322; 1988. *Jpn. J. Appl. Phys.* 27: L1587
27. Zhang, Z., Ye, H. Q., Kuo, K. H. 1985. *Philos. Mag.* A52: L49
28. Dong, C., Hei, Z. H., Wang, L. B., Song, Q. H., Wu, Y. K., Kuo, K. H. 1986. *Scr. Metall.* 20: 1155
29. Kelton, K. F., Gibbons, P. C., Sabes, P. N. 1988. *Phys. Rev. B* 38: 7810
30. Holzer, J. C., Kelton, K. F., Levine, L. E., Gibbons, P. C. 1989. *Scr. Metall.* 23: 691
31. Zhang, X., Kelton, K. F. 1990. *Philos. Mag. Lett.* 62: 265
32. Chen, H. S., Inoue, A. 1987. *Scr. Metall.* 22: 527
33. Kelton, K. F. 1989. *Phase Transit.* 16/17: 367
34. Schaefer, R. J., Bendersky, L. 1988. See Ref. 3, p. 111
35. Bendersky, L. A., Ridder, J. D. 1986. *J. Mater. Res.* 1: 405
36. Robertson, J. L., Moss, S. C., Kreider, K. G. 1988. *Phys. Rev. Lett.* 60: 2062
37. Chen, L. C., Spacpen, F. 1988. *Nature* 336: 366
38. Shen, Y., Poon, S. J., Shiflet, G. J. 1986. *Phys. Rev. B* 34: 3516
39. Tsai, A. P., Inoue, A., Bizen, Y., Masumoto, T. 1989. *Acta Metall.* 37: 1443
40. Holzer, J. C., Kelton, K. F. 1990. Preprint
41. Dubost, B., Lang, J. M., Tanaka, M., Sainfort, P., Audier, M. 1986. *Nature* 324: 48
42. Gayle, F. W. 1987. *J. Mater. Res.* 2: 1
43. Bartges, C., Tosten, M. H., Howell, P. R., Ryba, E. R. 1987. *J. Mater. Sci.* 22: 1663
44. Ohashi, W., Spacpcn, F. 1987. *Nature* 330: 555

45. Bancel, P. A. 1989. *Phys. Rev. Lett.* 63: 2741
46. Kittel, C. 1986. *Introduction to Solid State Physics*, p. 9. New York: Wiley
47. Guryan, C., et al. 1989. *Phys. Rev. Lett.* 62: 2409
48. Elser, V. 1986. *Phys. Rev. B* 32: 4892
49. Elser, V. 1986. *Acta Crystallogr. A* 42: 36
50. Bancel, P. A., Heiney, P. A., Stephens, P. W., Goldman, A. I., Horn, P. M. 1985. *Phys. Rev. Lett.* 54: 2422
51. Bak, P. 1985. *Phys. Rev. Lett.* 54: 1517; 1985. *Phys. Rev. B* 32: 5764
52. Duneau, M., Katz, A. 1985. *Phys. Rev. Lett.* 54: 2688
53. Janner, A., Janssen, T. 1977. *Phys. Rev. B* 15: 643
54. de Wolff, P. M. 1974. *Acta Crystallogr. A* 30: 777
55. Kalugin, P. A., Kitaev, A. Y., Levitov, L. S. 1985. *JETP Lett.* 41: 145
56. Kramer, P., Neri, R. 1984. *Acta Crystallogr. A* 40: 580
57. de Bruijn, N. G. 1981. *Proc. K. Ned. Akad. Wet.* A84: 39, 53
58. Levine, D., Lubensky, T. C., Ostlund, S., Ramaswamy, S., Steinhardt, P. J., Toner, J. 1985. *Phys. Rev. Lett.* 54: 1520
59. Lubensky, T. C., Socolar, J. E. S., Steinhardt, P. J., Bancel, P. A., Heiney, P. A. 1986. *Phys. Rev. Lett.* 57: 1440
60. Socolar, J. E. S., Wright, D. C. 1987. *Phys. Rev. Lett.* 59: 221
61. Cahn, J. W., Shechtman, D., Gratias, D. 1986. *J. Mater. Res.* 1: 13
62. Gahler, F., Rhyner, J. 1985. *Phys. Rev. Lett.* 55: 2369
63. Elser, V., Henley, C. L. 1985. *Phys. Rev. Lett.* 55: 2883
64. Audier, M., Guyot, P. 1986. *Philos. Mag. B* 53: L43
65. Rokhsar, D. S., Mermin, N. D., Wright, D. C. 1987. *Phys. Rev. B* 35: 5487
66. Mermin, N. D., Rokhsar, D. S., Wright, D. C. 1987. *Phys. Rev. Lett.* 58: 2099
67. Bak, P., Goldman, A. I. 1988. See Ref. 3
68. Devaud-Rzepski, J., Quivy, A., Calvayrac, Y., Cornier-Quiquandon, M., Gratias, D. 1989. *Philos. Mag. B* 60: 855
69. Ebalard, S., Spaepen, F. 1990. *J. Mater. Res.* 5: 62
70. Mukhopadhyay, N. K., Ranganathan, S., Chattopadhyay, K. 1987. *Philos. Mag. Lett.* 56: 121; 1989. *Philos. Mag. Lett.* 60: 207
71. Henley, C. L. 1988. *Philos. Mag. Lett.* 58: 87
72. Goldman, A. I., Guryan, C. A., Stephens, P. W., Parsey, J. M., Aeppli, G., et al. 1988. *Phys. Rev. Lett.* 61: 1962
73. Tsai, A. P., Chen, H. S., Inoue, A., Masumoto, T. 1991. *Phys. Rev. B* 43: 8782
74. Mukhopadhyay, N. K., et al. 1987. *J. Mater. Res.* 2: 299
75. Denoyer, F., Heger, G., Lambert, M., Lang, J. M., Sainfort, P. 1987. *J. Phys.* 48: 1357
76. Swamy, V. T., Ranganathan, S., Chattopadhyay, K. 1989. *J. Mater. Res.* 4: 539
77. Kelton, K. F., Gibbons, P. C., Sabes, P. N. 1988. *Phys. Rev. B* 38: 7810
78. Gibbons, P. C., Kelton, K. F., Levine, L. E., Phillips, R. B. 1989. *Philos. Mag. B* 59: 593
79. Jaric, M. V., Nelson, D. R. 1988. *Phys. Rev. B* 37: 4458
80. Ishii, Y. 1991. *Phys. Rev. B*. Submitted
81. Widom, M. 1991. *Phil. Mag. Lett.* Submitted
82. Gibbons, P. C., Kelton, K. F., Levine, L. E., Phillips, R. B. 1990. See Ref. 10, p. 516
83. Sastry, G. V. S., Suryanarayana, C., Van Tendeloo, G. 1982. *Phys. Status Solidi A* 73: 267
84. Shechtman, D., Schaefer, R. J., Biancaniello, F. S. 1984. *Metall. Trans. A* 15: 1987
85. Bendersky, L. 1985. *Phys. Rev. Lett.* 55: 1461
86. Chattopadhyay, K., et al. 1985. *Curr. Sci.* 54: 895
87. Bendersky, L., Schaefer, R. J., Biancaniello, F. S., Boettinger, W. J., Kaufman, M. J., Shechtman, D. 1985. *Scr. Metall.* 19: 909
88. Schaefer, R. J., Bendersky, L. 1986. *Scr. Metall.* 20: 745
89. Kuo, K. H. 1990. *J. Less Common Met.* 163: 9
90. Idziak, S., Heiney, P. A., Bancel, P. A. 1987. *Mater. Sci. Forum* 22-24: 353
91. He, L. X., Wu, Y. K., Kuo, K. H. 1988. *J. Mater. Sci. Lett.* 7: 1284
92. Kortan, A. R., Thiel, F. A., Chen, H. S., Tsai, A. P., Inoue, A., Masumoto, T. 1989. *Phys. Rev. B* 40: 9397
93. Steurer, W. 1989. *Acta Crystallogr. B* 45: 534
94. Ho, T. L. 1986. *Phys. Rev. Lett.* 56: 468
95. Koopmans, B., Schurer, P. J., van der Woude, F. 1987. *Phys. Rev. B* 35: 3005
96. Ishii, Y. 1990. See Ref. 12, p. 129; 1989. *Phys. Rev. B* 39: 11862
97. Choy, T. C., et al. 1988. *Philos. Mag. B* 58: 35
98. Aragon, J. L., et al. 1990. *Scr. Metall.* 24: 723
99. Mukhopadhyay, N. K., Chattopad-

- hyang, K., Ranganathan, S. 1991. See Ref. 7, p. 212
100. Fung, K. K., et al. 1986. *Phys. Rev. Lett.* 56: 2060
 101. Li, X. Z., Kuo, K. H. 1988. *Philos. Mag. Lett.* 58: 167
 102. Wang, N., et al. 1987. *Phys. Rev. Lett.* 59: 1951
 103. Wang, N., Kuo, K. H. 1989. *Philos. Mag. B* 60: 347
 104. Chen, H., Li, D. X., Kuo, K. H. 1988. *Phys. Rev. Lett.* 60: 1645
 105. Ishimasa, T., et al. 1985. *Phys. Rev. Lett.* 55: 511
 106. Kuo, K. H. 1989. *Int. J. Mod. Phys.* 3: 665
 107. Kuo, K. H. 1990. See Ref. 11, p. 92
 108. Ho, T. L., Li, Y. H. 1989. *Phys. Rev. Lett.* 62: 917
 109. Lequan, M., Yuzhen, W. 1990. *Phys. Rev. Lett.* 65: 3409
 110. He, L. X., Li, X. Z., Zhang, Z., Kuo, K. H. 1988. *Phys. Rev. Lett.* 61: 1116
 111. Lu, S. S., Chang, T. 1957. *Acta Sci. Sin.* 13: 150
 112. Amelinckx, S., Van Heurck, C., Van Tendeloo, G. 1991. See Ref. 7, p. 300
 113. Stephens, P. W., Goldman, A. I. 1986. *Phys. Rev. Lett.* 57: 2770
 114. Shaw, L. J., Elser, V., Henley, C. L. 1990. *Phys. Rev.* 43: 3423
 115. Hiraga, K., et al. 1985. *J. Phys. Soc. Jpn.* 54: 4077
 116. Guyot, P., Audier, M., Lequette, R. 1986. See Ref. 14, p. 389
 117. Knowles, K. M., et al. 1985. *Philos. Mag. B* 52: L31
 118. Reyes-Gasga, J., Van Tendeloo, G., Yacamán, M. J. 1991. See Ref. 10, p. 356
 119. Hiraga, K., Hirabayashi, M., Inoue, A., Masumoto, T. 1987. *J. Microsc.* 146: 245
 120. Burns, M. M., Fournier, J.-M., Golovchenko, J. A. 1990. *Sci. Am.* 263: 29
 121. Hiraga, K., et al. 1988. *Jpn. J. Appl. Phys.* 27: L951
 122. Kortan, A. R., Becker, R. S., Thiel, F. A., Chen, H. S. 1990. *Phys. Rev. Lett.* 64: 200
 123. Bergman, G., Waugh, J. L. T., Pauling, L. 1957. *Acta Crystallogr.* 10: 254
 124. Widom, M. 1988. See Ref. 3, p. 59
 125. Romeu, L. D. 1990. See Ref. 10, p. 140
 126. Audier, M., Guyot, P. 1990. See Ref. 11, p. 74
 127. Shoemaker, D. P., Shoemaker, C. B. 1988. See Ref. 3, p. 1
 128. Hiraga, K. 1990. See Ref. 12, p. 68
 129. Ohashi, W. 1990. PhD thesis. Harvard Univ., Cambridge, Mass.
 130. Spacop, F. 1990. See Ref. 11, pp. 1-18
 131. Henley, C. L. 1991. *Phys. Rev. B* 43: 993
 132. Chen, H., Burkov, S. E., He, Y., Poon, S. J., Shiflet, G. J. 1990. *Phys. Rev. Lett.* 65: 72
 133. Yamamoto, A., Kato, K., Shibuya, T., Takeuchi, S. 1990. *Phys. Rev. Lett.* 65: 1603
 134. Cahn, J. W., Gratias, D., Mozer, B. 1988. *J. Phys.* 49: 1225; 1988. *Phys. Rev. B* 38: 1638
 135. Qiu, S. Y., Jaric, M. V., Janot, C., de Boissieu, M. 1990. *Phys. Rev. Lett.* Submitted
 136. de Boissieu, M., et al. 1990. See Ref. 11, p. 109
 137. Lubensky, T. C. 1988. See Ref. 3, p. 199
 138. Ma, Y. J., Stern, E. A., Li, X. O. Janot, C. 1989. *Phys. Rev. B* 40: 8053
 139. Axe, J. D., Bak, P. 1982. *Phys. Rev. B* 26: 4963
 140. Ishii, Y. 1990. *Philos. Mag. Lett.* 62: 393; 1989. *Phys. Rev. B* 39: 1862
 141. Cullity, B. D. 1967. *Elements of X-Ray Diffraction*, Chap. 9. London: Addison-Wesley
 142. Heiney, P. A., Bancel, P. A., Horn, P. M., Jordan, J. L., LaPlaca, S., et al. 1987. *Science* 238: 660
 143. Levine, L. E., et al. 1990. Preprint
 144. Koskenmaki, D. C., Chen, H. S., Rao, K. V. 1986. *Phys. Rev. B* 33: 5328
 145. Audier, M., Sainfort, P., Dubost, B. 1986. *Philos. Mag. B* 54: L105
 146. Goldman, A. I., et al. 1990. See Ref. 11, pp. 60-73
 147. Field, R. D., Fraser, H. L. 1984. *Mater. Sci. Eng.* 68: L17
 148. Carr, M. J. 1986. *J. Appl. Phys.* 59: 1063
 149. Yang, C. Y. 1979. *J. Cryst. Growth* 47: 274
 150. Yang, C. Y., Yacamán, M. J., Heiney, P. A., K. 1979. *J. Cryst. Growth* 47: 283
 151. Shechtman, D. 1986. See Ref. 14, p. 1
 152. Denoyer, F., Heger, G., Lambert, M., Lang, J. M., Sainfort, P. 1987. *J. Phys.* 48: 1357
 153. Pauling, L. 1989. See Ref. 4, pp. 1-36
 154. Bancel, P. A., Heiney, P. A., Stephens, P. W., Goldman, A. I. 1986. *Nature* 319: 104
 155. Bancel, P., et al. 1989. *Proc. Natl. Acad. Sci. USA* 86: 8600
 156. Pauling, L. 1989. *Proc. Natl. Acad. Sci. USA* 86: 8595
 157. Hiraga, K., Sun, W., Lincoln, F. J. 1991. *Jpn. J. Appl. Phys.* 32: L302; 1991. *Mater. Trans. JIM* 32: 308
 158. Goldman, A. I., Shield, J. E., Guryan, C. A., Stephens, P. W. 1990. See Ref. 11, p. 60

159. Stephens, P. W., Goldman, A. I. 1986. *Phys. Rev. Lett.* 56: 1168; 57: 2331
160. Elser, V. 1987. In *Proceedings of the XVth International Colloquium on Group Theoretical Methods in Physics*, ed. R. Gilmore, D. H. Feng. Singapore: World Scientific; 1991. See Ref. 5, p. 105
161. Nori, F., Ronchetti, M., Elser, V. 1988. *Phys. Rev. Lett.* 61: 2774
162. Stephens, P. W. 1988. See Ref. 4, p. 37
163. Robertson, J. L., Moss, S. 1991. *Z. Phys. B*. In press; 1991. *Phys. Rev. Lett.* 66: 353
164. Levine, D., Steinhart, P. J. 1984. *Phys. Rev. Lett.* 53: 2477; 1986. *Phys. Rev. B* 34: 596
165. Socolar, J. E. S., Steinhart, P. J. 1986. *Phys. Rev. B* 34: 3345
166. Gardner, M. 1977. *Sci. Am.* 236(1): 110
167. Grunbaum, B., Shepard, G. C. 1987. *Tilings and Patterns*. New York: Freeman
168. Penrose, R. 1988. See Ref. 4, p. 53
169. Onoda, G. Y., Steinhart, P. J., DiVincenzo, D. P., Socolar, J. E. S. 1988. *Phys. Rev. Lett.* 60: 2653; 1989. *Phys. Rev. Lett.* 62: 1210
170. Jaric, M. V., Ronchetti, M. 1989. *Phys. Rev. Lett.* 62: 1209
171. Burkov, S. E. 1988. *J. Stat. Phys.* 52: 453
172. Widom, M., Strandburg, K. J., Swendsen, R. H. 1986. *Phys. Rev. Lett.* 58: 706
173. Leung, P. W., Henley, C. L., Chester, G. V. 1989. *Phys. Rev. B* 39: 446
174. Lancon, F., Billard, L., Chaudhari, P. 1986. *Europhys. Lett.* 2: 625
175. Lancon, F., Billard, L. 1988. *J. Phys.* 49: 249
176. Henley, C. L. 1990. See Ref. 12
177. Henley, C. L. 1988. *J. Phys. A* 21: 1649
178. Shaw, L. J., Henley, C. L. 1991. *J. Phys. A*. Submitted
179. Widom, M., Deng, D. P., Henley, C. L. 1989. *Phys. Rev. Lett.* 63: 310
180. Strandburg, K. J., Tang, L., Jaric, M. V. 1989. *Phys. Rev. Lett.* 63: 314
181. Henley, C. L. 1991. See Ref. 7
182. Henley, C. L. 1990. See Ref. 10, p. 152
183. Widom, M. 1990. See Ref. 11, p. 337
184. Li, W., Park, H., Widom, M. 1990. *J. Stat. Phys.* 61: 51
185. Biham, O., Mukamel, D., Shtrikman, S. 1988. See Ref. 3, p. 171
186. Aragon, J. L., Reyes-Gasga, J., Jose-Yacamán, M. 1990. *Philos. Mag. Lett.* 62: 337
187. Kawamura, H. 1986. *Prog. Theor. Phys.* 70: 352
188. Villars, P., Hulliger, F. 1987. *J. Less Common Met.* 132: 289
189. Villars, P., Phillips, J. C., Chen, H. S. 1986. *Phys. Rev. Lett.* 57: 3085
190. Chen, H. S., Phillips, J. C., Villars, P., Kortan, A. R., Inoue, A. 1987. *Phys. Rev. B* 35: 9326
191. Rabe, K. M., Kortan, A. R., Phillips, J. C., Villars, P. 1991. *Phys. Rev. B* 43
192. Kohmoto, M., Sutherland, B., Tang, C. 1987. *Phys. Rev. B* 35: 1024
193. Niu, Q., Nori, F. 1986. *Phys. Rev. Lett.* 57: 1467
194. Sokoloff, J. B. 1985. *Phys. Rep.* 126: 189
195. Simon, B. 1982. *Adv. Appl. Math.* 3: 463
196. Ostlund, S., Pandit, R. 1984. *Phys. Rev. B* 29: 1394
197. Sokoloff, J. B. 1986. *Phys. Rev. Lett.* 57: 2223
198. Biggs, B. D., Poon, S. J., Munirathnam, N. R. 1990. *Phys. Rev. Lett.* 65: 2700
199. Mott, N. 1987. *Conduction in Non-Crystalline Materials*. New York: Oxford
200. Wagner, J. L., Biggs, B. D., Poon, S. J. 1990. *Phys. Rev. Lett.* 65: 203
201. Fujiwara, T. 1989. *Phys. Rev. B* 40: 942
202. Fujiwara, T., Yokokawa, T. 1990. See Ref. 12, p. 196; 1991. *Phys. Rev. Lett.* 66: 333
203. Phillips, R. B., Carlsson, A. E. 1988. *Phys. Rev. B* 37: 10880; 1990. *Phys. Rev. B* 42: 3345
204. Smith, A. P., Ashcroft, N. W. 1987. *Phys. Rev. Lett.* 59: 1365
205. Vaks, V. G., Kamysenko, V. V., Samolyuk, G. D. 1988. *Phys. Lett. A* 132: 131
206. Friedel, J. 1988. *Helv. Phys. Acta* 61: 538
207. Carlsson, A. E., Phillips, R. B. 1991. See Ref. 7
208. Bancel, P. A., Heiney, P. A. 1986. *Phys. Rev. B* 33: 7917
209. Miceli, P. F., Youngquist, S. E., Neumann, D. A., Zabel, H., Rush, J. J., Rowe, J. M. 1986. *Phys. Rev. B* 34: 8977
210. Suck, J.-B., Bretscher, H., Rudin, H., Grutter, P., Guntherodt, H. J. 1987. *Phys. Rev. Lett.* 59: 102
211. Merlin, R., Bajema, K., Clarke, R., Juang, F. V., Bhattacharya, P. K. 1985. *Phys. Rev. Lett.* 55: 1768
212. Nakayama, M., Hato, H., Nakashima, S. 1987. *Phys. Rev. B* 36: 3472
213. Niu, Q., Nori, F. 1989. *Phys. Rev. B* 39: 2134
214. Behrooz, A., et al. 1986. *Phys. Rev. Lett.* 57: 368
215. He, S., Maynard, J. D. 1989. *Phys. Rev. Lett.* 62: 1888

216. Suck, J.-B., et al. 1990. In *Phonons '89*, Vol. 1, ed. S. Hunklinger, W. Ludwig, G. Weib, p. 576. Singapore: World Scientific
217. Birge, N. O., et al. 1987. *Phys. Rev. B* 36: 7685
218. Goldman, A. I., et al. 1990. *Phys. Rev. B* 43: 8763
219. Quilichini, M., Heger, G., Hennion, B., Lefebvre, S., Quivy, A. 1990. *J. Phys.* 51: 1785
220. Reynolds, G. A. M., et al. 1990. *Phys. Rev. B* 41: 1194
221. Ashraff, J. A., Stinchcombe, R. B. 1989. *Phys. Rev. B* 39: 2670
222. Ashraff, J. A., Luck, J.-M., Stinchcombe, R. B. 1990. *Phys. Rev. B* 41: 4314
223. Benoit, C., Possigue, G., Azougarh, A. 1990. *J. Phys. Condens. Matter* 2: 2519
224. Patel, H., Sherrington, D. 1989. *Phys. Rev. B* 40: 11185
225. Widom, M. 1985. *Phys. Rev. B* 31: 6456
226. McHenry, M. E., Eberhart, M. E., O'Handley, R. C., Johnson, K. H. 1986. *Phys. Rev. Lett.* 56: 81
227. Hauser, J. J., Chen, H. S., Waszczak, J. V. 1986. *Phys. Rev. B* 33: 3577
228. Youngquist, S. E., et al. 1986. *Phys. Rev. B* 34: 2960
229. Hauser, J. J., et al. 1986. *Phys. Rev. B* 34: 4674
230. Warren, W. W., Chen, H.-S., Espinosa, G. P. 1986. *Phys. Rev. B* 34: 4902
231. McHenry, M. E., et al. 1989. *Phys. Rev. B* 39: 3611
232. Edagawa, K., et al. 1987. *J. Phys. Soc. Jpn.* 56: 2629
233. Eibschutz, M., et al. 1987. *Phys. Rev. Lett.* 59: 2443
234. Bennett, L. H., Rubinstein, M., Xiao, G., Chien, C. L. 1987. *J. Appl. Phys.* 61: 4364
235. Stadnik, Z. M., Stroink, G. 1988. *Phys. Rev. B* 38: 10447
236. Stadnik, Z. M., et al. 1989. *Phys. Rev. B* 39: 9797
237. Machado, F. L. A., et al. 1987. *Solid State Commun.* 61: 145, 691
238. Bellissent, R., Hippert, F., Monod, P., Vigneron, F. 1987. *Phys. Rev. B* 36: 5540
239. Berger, C., et al. 1988. *Phys. Rev. B* 37: 6525
240. Wong, K. M., Poon, S. J. 1986. *Phys. Rev. B* 34: 7371
241. Dunlap, R. A., McHenry, M. E., Srinivas, V., Bahadur, D., O'Handley, R. C. 1989. *Phys. Rev. B* 39: 4808
242. Tsai, A. P., et al. 1988. *Jpn. J. Appl. Phys.* 27: L2252
243. Stadnik, Z. M., Stroink, G. 1991. *Phys. Rev. B* 43: 894
244. Lubensky, T. C., Tokihiro, T., Renn, S. R. 1990. *Phys. Rev. Lett.* 67: 89
245. Anonymous. 1990. *Fr. Adv. Sci. Technol.* 4: 3